Stony Brook University

Hydrophobically modified glycol chitosan nanoparticles for targeting breast cancer microcalcification using alendronate probes

A Thesis Presented

by

Kamalakannan Vishnu

to

The Graduate School

in Partial Fulfillment of the

Requirements

for the Degree of

Master of Science

in

Material Science and Engineering

Stony Brook University

May 2017

Stony Brook University

The Graduate School

Kamalakannan Vishnu

We, the thesis committee for the above candidate for the

Master of Science degree, hereby recommend

acceptance of this thesis.

Yizhi Meng – Thesis Advisor
Assistant Professor, Material Science and Engineering

T Venkatesh – Committee member
Associate Professor and Graduate program director, Material Science and Engineering

Gábor Balázsi – Committee member
Henry Laufer Endowed Associate Professor, Department of Biomedical Engineering

This thesis is accepted by the Graduate School

Charles Taber
Dean of the Graduate School

Abstract of the Thesis

Hydrophobically modified glycol chitosan nanoparticles for targeting breast cancer microcalcification using alendronate probes

by

Kamalakannan Vishnu

Master of Science

in

Material Science and Engineering

Stony Brook University

2017

In 2016, invasive breast cancer was diagnosed in about 246,660 women and 2,600 men. An additional 61,000 new cases of in situ breast cancer was diagnosed in women. Microcalcifications are most common abnormalities detected by mammography for breast cancer, present in about 30% of all malignant breast lesions. Tumor specific biomarkers are used for targeting these abnormalities. Nanoparticles with multimodal and combinatorial therapies and conjunction of bio-ligands for specific molecular targeting using surface modifications effectually deliver a variety of drugs and are simultaneously used to image tumor progression. Alendronate, a germinal bisphosphonate conjugation as a targeting ligand would improve the nanoparticle's direct binding to hydroxyapatite (HA) mimicking calcified spots in breast cancer lesions. In this study, the hydrophobically modified glycol chitosan (HGC) micelle was modified with alendronate surface functionalization using a biotin-avidin interaction to improve the nanomicelle's calcification targeting ability. Biotinylated, avidinlyated hydrophobically modified

glycol chitosan particles were linked to biotinylated alendronate via a strong biotin-avidin linkage. Cyanine 3, a red fluorescent dye was conjugated to the amine groups on HGC for visualization of micelles. The size of the nanoparticles measured was 254.0 ± 0.43 nm and 209.7 ± 1.0 nm for Cy3-BHGCA and Cy3-BHGCA-BALN nanoparticles respectively. The average surface charge was measured to be +26.9 ± 0.19 mV and +27.68 ± 0.20 mV for Cy3-BHGCA and Cy3-BHGCA-BALN nanoparticles respectively. Binding affinity using hydroxyapatite (HA) revealed that both Cy3 BHGCA BALN and Cy3 BHGCA nanoparticles displayed 95% binding in 24 hours. However, the biotin quenched nanoparticle Cy3 BHGCAB displayed 68% binding in 24 hours. The synthesis and binding chemistry was verified using Fourier transform infrared spectroscopy (FTIR).

Table of Contents

List of Figures……..x

List of Tables……..……xiii

List of Abbreviations…….……xiv

Acknowledgements……..…….....xvi

Chapter 1: Introduction ……...……1

1.1 Cancer ……..……...1

1.1.1 Therapy and Diagnostics……..……2

1.1.2 Targeted Theranostics……..……3

1.2 Micelles……..…….....4

1.3 Chitosan based nanoparticles……..……6

1.3.1 Drug delivery application……..……...7

1.3.2 Hydrophobically modified glycol chitosan……..……..……...8

1.3.3 Factors influencing carrier properties……..……9

1.3.4 Promising carrier applications……..…….....10

1.4 Breast Cancer ……..…….……10

1.4.1 Breast cancer microcalcifications……..……...……..11

1.4.2 Microcalcifications as target……..……...……11

1.5 Bisphosphonates……..……12

1.5.1 Alendronate……..……13

1.6 Avidin-Biotin interactions…….……..…….……14

1.6.1 HABA assay……...……...……..……16

1.7 Fluorescence labelling……...……...16

1.8 Particle characterization……..……..……17

Chapter 2: Objective.……..……18

Chapter 3: Materials and Methods.……20

3.1 Materials……..……..……20

3.2 Nanoparticle Synthesis……..……21

3.2.1 Synthesis of HGC nanoparticles……..……21

3.2.1.1 Biotinylation of Glycol Chitosan……..…….21

3.2.1.2 Biotin Quantification – Biotinylation Level……..……...23

3.2.1.3 Biotin Quantification HABA assay……...……...23

3.2.1.4 Avidinylation of BGC……...24

3.2.1.5 Hydrophobic modification of NPs with 5ß cholanic acid…….....24

3.2.1.6 Cy3 labeling of nanoparticles……...26

3.2.2 Preparation of alendronate functionalized nanoparticles……...….27

3.2.2.1 Biotinylation of Alendronate…….…….28

3.2.2.2 Alendronate conjugation and Cy3 labeling of nanoparticles……29

3.2.2.3 Biotin quenching of Cy3 BHGCA nanoparticle……...30

3.2.3 Preparation of nanoparticle suspension……..30

3.3 Particle size and zeta potential measurements…….……30

3.4 Binding affinity studies……31

3.5 FTIR analysis……...……32

3.5.1 Air-drying the sample for FTIR……..32

3.5.2 FTIR experimental setup……...……..32

Chapter 4 Results……...……34
4.1 Nanoparticle synthesis…….…….34
4.1.1 Biotinylation efficiency……..34
4.1.2 Cy3 Labeling…….……..35
4.2 Size and zeta potential…….…….38
4.3 Binding affinity towards HA……...…….39
4.4 FTIR analysis……...…….47
4.5 Additional Experiments……...…….51
4.5.1 Preparation of DOXO loaded HGC……..……..51
4.5.1.1 Preparation of doxorubicin solution…….....52
4.5.1.2 Standard curve of DOXO in DMSO:HCl (10:2, v/v)……..…….53
4.5.1.3 Standard Curve of DOXO in PBS……...…….54
4.5.1.4 Encapsulation efficiency…….…….……54
4.5.2 DOXO release kinetics……...…….56
4.5.3 Delivery of DOXO-loaded HGC nanoparticles to 4T1 murine carcinoma cells……..57
4.5.3.1 Preparing Cell Culture Medium for 4T1 murine carcinoma cells……..57
4.5.3.2 Cell Plating……...…….57
4.5.3.2 Adding Nanoparticles to the plated cells…….…….58
4.5.3.3 Freezing of cells……...…….58
4.5.3.4 Cytotoxicity study: MTS assay…….59
Chapter 5 Discussion ……62

5.1 Physiochemical properties……..……...62

5.2 Size and Zeta potential results……..63

5.3 Binding affinity……...……..64

5.4 FTIR analysis……..……..65

Chapter 6: Conclusion ……...……67

Chapter 7: Future work ……..……69

Chapter 8. Reference ……..……70

List of Figures

Figure 1: Micelle structure……...5

Figure 2. Glycol chitosan chemical structure.……...8

Figure 3. Alendronate chemical.…….13

Figure 4. Biotin avidin interaction schematic…….15

Figure 5. Synthesis of HGC nanoparticles flow diagram……...…….21

Figure 6. Chemical Synthesis of Biotinylation of glycol chitosan- a) Glycol chitosan was reacted with b) Sulfo-NHS-LC Biotin to give c) Biotinylated glycol chitosan……..….22

Figure 7. Chemical Synthesis of Hydrophobically modified Avidin-Biotinylated glycol chitosan a) Avidin-Biotinylated Glycol chitosan was conjugated with b) 5ßcholanic acid to give c) Hydrophobically modified glycol chitosan……25

Figure 8. Cyanine 3 was attached to the amine group of chitosan to Cy3 labelled BHGCA nanoparticles……..……26

Figure 9. Experimental design for making BHGCA-BALN nanoparticle……..…27

Figure 10. Chemical Synthesis of Biotinylated alendronate- a) Alendronate was reacted with b) Sulfo-NHS-LC Biotin to give c)Biotinylated alendronate BALN…….28

Figure 11. Biotinylated alendronate was conjugated and Cyanine 3 was attached to the amine group of chitosan to Cy3 labelled BHGCA nanoparticles……..……29

Figure 12. UV-Vis absorbance scan of a) ALN in HPLC water vs plain HPLC water, b) ALN in DMSO and plain DMSO……36

Figure 13. Standard concertation curve for a) Cy3-BHGCA-BALN b) Cy3-BHGCA c) Cy3 BHGCA Biotin prepared in water…..……37

Figure 14. Binding affinity of Cy3-BHGCA and Cy3-BHGCA-BALN nanoparticles towards different mass of HA 10mg, 20mg, 30m...……40

Figure 15. a) Binding affinity of Cy3-BHGCA nanoparticles towards different mass of HA 50mg, 100mg, 200mg……...……....…….……41

Figure 16. Binding affinity of Cy3-BHGCA-BALN nanoparticles towards different mass of HA 50mg, 100mg, 200mg.……...……42

Figure 17. Binding affinity of Cy3-BHGCA and Cy3-BHGCA-BALN nanoparticles towards different mass of HA a) 50mg b) 100mg c) 200mg……...……44

Figure 18. Binding affinity of Cy3-BHGCA-Biotin nanoparticles towards different mass of HA 50mg, 100mg, 200mg……45

Figure 19. Binding affinity of Cy3-BHGCA BALN and Cy3-BHGCA-Biotin nanoparticles towards different mass of HA a) 50mg b) 100mg c) 200mg….……46

Figure 20. FTIR spectrum of a) Alendronate only and b) Biotinylated alendronate…….……47

Figure 21. FTIR spectrum of a) Cy3 HGC, b) Cy3 BHGCAB and c) Cy3 BHGCA BALN nanoparticles.…….……48

Figure 22. FTIR spectrum of Cy3 BHGCAB nanoparticles in HA studies. Comparison of a) Hydroxyapatite only, b) Cy3 BHGCAB NP only c) Physical mix of a and b d) chemically bound a and b...……..49

Figure 23. FTIR spectrum of Cy3 HGC nanoparticles in HA studies. Comparison of a) Hydroxyapatite only, b) Cy3 HGC NP only c) Physical mix of a and b d) chemically bound a and b.…..……..50

Figure 24. FTIR spectrum of Cy3 BHGCA BALN nanoparticles in HA studies. Comparison of a) Hydroxyapatite only, b) Cy3 BHGCA BALN NP only c) Physical mix of a and b d) chemically bound a and b.…….51

Figure 25. Standard curve DOXO in DMSO:HCl (10:2, v/v)……..…….53

Figure 26. Standard concentration curve for a) PBS pH b) 7.4 Phosphate Buffer pH 6.5……54

Figure. 27. Cumulative release of doxorubicin from HGC at pH 7.4……...…….56

Figure. 28. Cumulative release of doxorubicin from HGC at pH 6.5…...……...……..57

Figure 29. MTS data plots: Day 1 cells were treated with two different treatments - HGC-DOXO, and free DOXO as a control. Free DOXO and HGC/dendrimer begin to show signs of cell cytotoxicity around 10µM. HGC exhibits cell cytotoxicity around 30µM. Overall, cells were still relatively intact.…….……..60

Figure 30. Morphology study imaging showing fluorescence microscopy images of 4T1 cells after 1, 2 or 3 days of incubation with either free doxorubicin or DOXO-loaded nanoparticles. Untreated cells were used as control. Cells were visualized in the blue (nuclei) and green (cytoskeleton) channels.…….....……61

List of Tables

Table 1. Biotinylation efficiency……..……..35

Table 2. Size and zeta potential of Cy3-BHGCA and Cy3-BHGCA-BALN nanoparticle……...39

Table 3. Molar ratios for binding affinity of Cy3-BHGCA and Cy3-BHGCA-BALN nanoparticles towards different mass of HA 10mg, 20mg, 30mg...……..40

Table 4. Binding affinity data of Cy3-BHGCA nanoparticles towards different mass of HA…..41

Table 5. Binding affinity data Cy3-BHGCA-BALN nanoparticles towards different mass of HA…….……43

Table 6. Molar ratios for binding affinity of Cy3-BHGCA and Cy3-BHGCA-BALN nanoparticles towards different mass of HA 10mg, 20mg, 30mg…….……43

Table 7. Yield efficiency assessments for DOXO HGC encapsulation…….……52

Table 8. Encapsulation efficiency of DOXO encapsulated HGC nanoparticles at 1:10 and 1:15 (DOXO:HGC) ratios..……55

List of Abbreviations

HA	Hydroxyapatite
HGC	Hydrophobically modified glycol chitosan
CT	Computed tomography
MRI	Magnetic resonance imaging
EPR	Enhanced permeability and retention
DOXO	Doxorubicin
CMC	Critical Micelle Concentration
DS	Degree of substitution
TEM	Transmission electron microscopy
DLS	Dynamic light scattering
NMR	Nuclear magnetic resonance
PLGA	Poly Lactic-co-Glycolic Acid
PLA	Polylactic acid
^{H}NMR	hydrogen-1 NMR
FTIR	Fourier transform infrared spectroscopy
CNP	Chitosan nanoparticles
BP	Bisphosphonates
ALN	Alendronate
BALN	Biotinylated alendronate
RES	Reticuloendothelial system
SPIO	Supraparamagnetic oxide

HABA	4'-hydroxyazobenzene-2-carboxylic acid
Cy3	Cyanine 3
GC	Glycol chitosan
BGC	Biotinylated Glycol Citosan
BGC-A	Avidinylated BGC
BHGC-A	Hydrophobically modified BGC-A
EDC	1-Ethyl-3- (3-dimethylaminopropyl) carbodiimide hydrochloride
DMAP	4-(Dimethylamino)pyridine
DMEM	phenol red-free Dulbecco's Modified Eagle Media
MWCO	Mlecular weight cutoff
PBS	Phosphate buffer saline
HRP	Horseradish Peroxidase
MTS	3-(4,5-dimethylthiazol-2-yl)-5-(3-carboxymethoxyphenyl)-2-(4-sulfophenyl)-2H-tetrazolium

Acknowledgments

The person I would like to thank first is my advisor Dr. Yizhi Meng. She has provided me guidance and support for my academic study and my thesis. Her commitment to research and enthusiasm always inspired me. Thank you for encouraging me and supporting me in these two years.

I express my sincere gratitude to the members of my committee. I am especially thankful to Dr. Gábor Balázsi for his scientific knowledge and insightful comments. I would also thank Dr.T. Venkatesh for his support and insights.

I would like to express my thanks to Shelagh Zegers from the school of Marine and Atmospheric Sciences for her kind technical assistance with lyophilization. I am thankful to Dr.Dmytro Nykypanchuk and Dr. Fang Lu at Center for Functional Nanomaterials of Brookhaven National Laboratory for the experiment instrument training.

Many thanks to my lab colleague Weiyi Li for her assistance with the cell work. She introduced me to nanoparticles and helped me a lot with nanoparticles synthesis. I also express my gratitude to all my Laboratory members for their kindness and support.

Last but not least, I would like to thank my parents, Vishnu and Punitha. They worked so hard to support my life and study here. They are the very source of my strength.

Chapter 1: Introduction

1.1 Cancer

Cancer is a collection of diseases characterized by the uncontrolled growth and extent of abnormal cells, uncontrolled spread of which can result in death[1]. In 2016, 1,685,210 new cancer cases and 595,690 cancer-related deaths were projected to occur in the United States[1,2]. Both more and less economically developed countries experience the burden constituted by cancer. Risk elements that increase occurrences include but not limited to, smoking, overweight, physical inactivity and changing reproductive pattern.[3]

Ability to sustain chronic proliferation is the most fundamental trait of cancer cells. While normal cells carefully control production and release of signals for cell growth and division, to maintain tissue architecture and functions. Cancer cells initiate, drive and progress forward carrying oncogenic and tumor specific mutations making cancer a genetic disease.[4]

Advancing the fight against cancer will require continued clinical and basic research, which is dependent on the application of existing cancer control knowledge across all segments of the population[2]. Research on delivery and targeting of tumor, therapeutic, and diagnostic agents is at the forefront of projects in cancer nanomedicine involving identification of precise targets by specific conditions and choice of the appropriate nanocarriers to accomplish the required responses while minimizing side effects[5].

1.1.1 Therapy and Diagnostics

The conventional strategies commonly employed to combat cancer include surgery, chemotherapy, radiotherapy, stem cell transplant therapy, immunotherapy, and various targeted therapies. Surgical interventions have always been a widespread mode of cancer treatment, yet limited by recurrent post-surgery relapse often demands adoption of adjuvant therapies, such as chemotherapy and radiotherapy (or both)[6]. It was Chemotherapy that eventually led to the identification of most of the new drug targets that are currently the focus of cancer drug development, transitioning to the age of "targeted therapy". The first and best example of targeted therapy is the development of the Bcr-Abl tyrosine kinase inhibitor imatinib for the treatment of chronic myelocytic leukemia.[7] In the United States, there has been a steady rise in the use of diagnostic radiologic procedures, especially x rays. Radiation treatment for benign disease was relatively common from the 1940's to the 1960's. As more was learned about radiation associated cancer risks and new treatments became available, the use of radiotherapy for benign disease has declined.[8] Despite significant evolution in cancer therapeutics, their toxic side effects are of paramount concern. Chemotherapy drugs, for example, might cause osteoporosis, infertility, premature ovarian failure, typhlitis, herpesviridae infections, hair loss, diarrhea and constipation.[6]

Over years, scientists have advanced strategies for effective diagnosis of abnormal growth and the presence of any tumor, as well as the reappearance of the tumors and the stage of their malignancies. For example, a computed tomography (CT) scan. Other systems for diagnosis include ultrasound, x-ray, magnetic resonance imaging (MRI), nuclear scan and most importantly biopsy (with the collection of a tissue or fluid sample, via needle, endoscope or surgery).[6]

1.1.2 Targeted Theranostics

A very important challenge treating cancer in general is to find a means for controlled targeted drug delivery and release. Modern research attempts to address this fundamental challenge by using nanoparticles as delivery vehicles. Nanoparticles, due to their unique size, wide shape variation to accommodate various drugs and biomolecules, and ability to incorporate specific targets and surface modification adding various functionality, meet a wide range of requirements for overcoming biological barriers.[6,9]

This amalgamation of therapy and diagnosis is known as 'theranostics'. Multimodal and combinatorial therapies and conjunction of bio-ligands for specific molecular targeting by virtue of their surface modifications and 'enhanced permeability and retention' (EPR) effect, various factions of nanoparticles that are Magnetic, Gold and silver-based, Graphene-based, Silica-based, Lipid- and polymer-based, Protein-based, can effectually deliver a variety of targeting agents (such as peptides, monoclonal antibodies, nucleic acids, chemotherapeutics etc.) to cancer cells. Simultaneously, used to image tumor progression by using MRI, fluorescence or other optical methods. These nanomedicine formulations aim to improve the biodistribution and target sites accumulation of systemically administered (chemo)therapeutic agents.[10] For example a mitochondrion-targeted self-delivery system of PpIX-PEG-$(KLAKLAK)_2$ (designated as PPK) exhibited high drug loading efficacy as well as dual-stage-light-guided tumor inhibition, with a short time light irradiation, PpIX enhanced the cellular internalization of PPK due to "photochemical internalization" (PCI) effect.[11] Similarly, multifunctional polymeric vehicle was prepared by single emulsion evaporation method, using carboxyl-terminated PLGA with LHRH as a targeting moiety on the surface of polymeric carrier by applying polyethylene glycol.[12]

These also include targeted contrast agents that improve the resolution of cancer cells to the single cell level, and nanodevices capable of addressing the biological and evolutionary diversity of the multiple cancer cells that make up a tumor within an individual.[10,13]

1.2 Micelles

One-third of drugs in development are water insoluble such as doxorubicin (DOX), paclitaxel (PTX) or camptothecin (CPT). Other hurdles include poor pharmacokinetics[14] and need to simultaneously overcome the membrane-associated multidrug resistance and the intracellular drug resistance. Block copolymer micelles improves effective solubility[15] by preventing the core enclosing the drug from interacting with the environment, enhances loading capacity for drugs as well as their unique disposition characteristics in the body[16] and end-group functionalization increases the targeting efficiency[17].

Micelle structures with highly branched nonporous interior could carry the desired drug and deliver to a target effectively. Micelles are aggregate or supramolecular assembly of surfactant molecule dispersed in liquid colloid. A typical micelle structure is formed as an aggregate with hydrophilic head in contact with surrounding solvent with hydrophobic single tail region towards micelle center by a process called micellization[18]

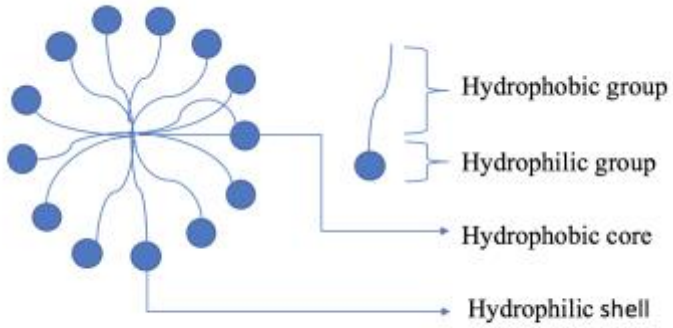

Figure 1: Micelle structure (drawn using MS Powerpoint)

Concentration of surfactant above which the micelles form and all surfactants added to the system is called Critical Micelle Concentration (CMC). When compared to conventional surfactant, Polymeric structures possess low CMC, stable aggregates, blocks with different chemical composition at the core and periphery of micelles[19] and have a slower rate of dissociation, allowing retention of loaded drugs for a longer period. For the design of micellar carrier systems for receptor-mediated drug delivery, the functionalization of its outer surface to modify its physicochemical and biological properties posts great value[15], while they lack flexibility and has broad molecular weight of building blocks giving rise to broad size distribution. These mechanisms negatively affect the complexation and release capabilities, thus hampering quantitative evaluation.

Unimolecular micelles seem to avoid the problem with highly branched (dendritic), organized, ever increasing functional group within the structures.[19] As for homopolymers, the chemical modification of a given block, for instance, by hydrogenation, halogenation, hydrolysis, etc. gives access to new types of copolymers.[17] Self-assembly of block copolymers in solution is driven by the different affinity, also referred to as block selectivity.[15] CMC is inversely

proportional to degree of substitution (DS) of hydrophobic component. For example in case of HGC, mean diameter of the aggregate decreases with increase in DS of 5β Cholanic acid its hydrophobic part because of formation of compact hydrophobic inner core[20], thus the specific size and morphology of such self-assembled structures is driven largely by thermodynamic forces.

Polymeric micelles have been shown to target tumor tissues, both because of passive accumulation through tumors' enhanced permeability and retention (EPR) effect and through deliberate active targeting using ligands, such as folic acid, and antibodies[15].

Examples of other biocompatible polymers that have been investigated to act as the hydrophilic corona (shell) include Poly (ethylene glycol) (PEG), poly (N-vinyl pyrrolidone) (PVP)[21], poly (2-ethyl-2-oxazoline) (PEOz)[22], and phosphocholine-based polymers[23]. The physical methods for the characterization of block copolymer micellar systems include TEM for Shape, size; DLS for hydrodynamic radius (R_h); Ultracentrifugation for Micelle density, molecular weight (Z average), micelle/unimer weight ratio; Fluorescence techniques for Chain dynamics, CMC, hybridization of micelles; NMR for Chain dynamics; Viscometry for R_h, intrinsic viscosity, Stop flow techniques for Kinetics of micelle formation and dissociation[17].

1.3 Chitosan based nanoparticles

Nanoencapsulation of drugs on biodegradable nanoparticles such as Poly Lactic-co-Glycolic Acid (PLGA), Polylactic acid (PLA), chitosan, gelatin, polycaprolactone and poly-alkyl-cyanoacrylates are frequently used to improve the therapeutic value. Several drug/bioactive molecules are successfully encapsulated improving bioactivity, bioavailablity and controlled delivery.[24] Marine organisms are of significant interest in recent years for its potential as a source of compounds with pharmacological benefits. Chitosan is a polysaccharide made by deacetylation

of crustacean exoskeleton (shells) with alkaline substance. Chitosan has an added advantage to deliver drug through skin and blood clotting capability. [25]

1.3.1 Drug delivery application

Chitosan based nanoparticles are being rigorously studied for the past decade for its array of application as an excellent candidate for drug delivery vehicle for various compounds on different formats, better efficiency than microsized vehicles and delivery cargo, more cellular internalization, stability and ability to be modified with application based functionality.[26] This is due to many functional groups that allow chemical modification using cross linking agents.[25] While size plays a role in internalization, its targeting efficiency is dependent on the targeted tissue. Physical loading and chemical conjugation are two methods for loading hydrophobic drug. Chemical conjugation of allows the chitosan polymer to form a spherical nanoparticle with a hydrophobic drug with increased stability and decreased frequency of unintended release.[27] Chitosan is interesting over other biopolymers due to its most critical features of biocompatibility, solubility and biodegradability which makes it perfect to be used for drug delivery application. Clearance by reticuloendothelial systems is retarded and longer in vivo residency time of delivery of encapsulated material play key roles for in vivo and in vitro drug and gene delivery.[26] The second fold of its advantage includes accumulation of nanoparticles in tumoral tissue owing to impaired lymphatic drainage resulting in a higher drug concentration at tumor site.[26]

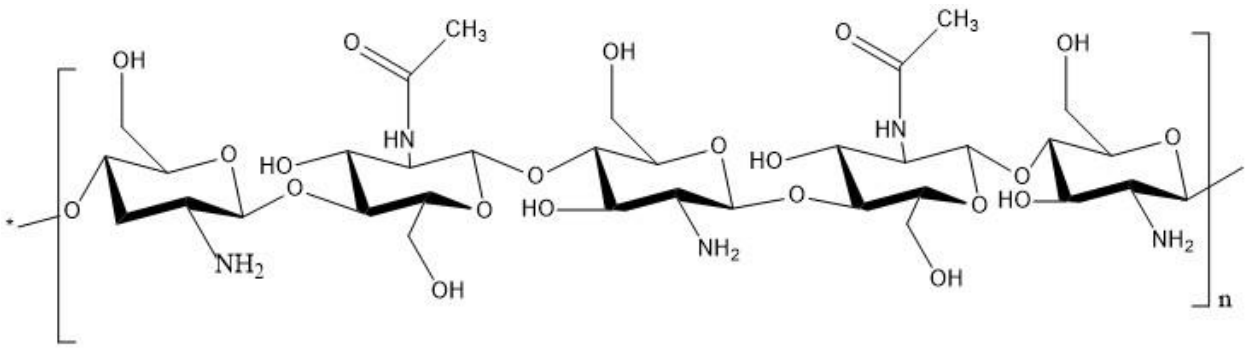

Figure 2. Glycol chitosan chemical structure (drawn using Chemdraw).

Chitosan nanoparticles are excellent candidates for oral delivery that are limited by poor permeation across gastrointestinal mucosa[28], by adhering to the walls of gastrointestinal track and its cationic nature facilitates electrostatic interaction with cell membrane affecting positively the biodistribution. They even facilitate delivery of peptides as leucine enkephalin across Blood brain barrier.[28] The degradation is carried out through enzymatic hydrolysis of chitinases, chitosanases and other nonspecific enzymes like lysozymes into chitin oligomers and monomers.[26]

1.3.2 Hydrophobically modified glycol chitosan

Glycol chitosan is a commercially available derivative of chitosan possessing enhanced water solubility majorly used as scaffolds for drug delivery and diagnostic imaging.[29] Nano sized synthetic particles like liposomes, micelles and oil in water emulsions have attracted great attention as potential drug delivery system.[30] Self-assembled nanoparticle based on Glycol chitosan bearing 5β Cholanic acid have been previously studied for its characteristics as a drug delivery vehicle. Hydrophobically modified glycol chitosan (HGC) results from a covalent bond between Glycol chitosan and 5β Cholanic acid which is the hydrophobic component. HGC forms self-aggregates by intra and intermolecular association between 5β Cholanic acid at random free amine groups attached to glycol chitosan at aqueous media. Previous studies involving investigation of

physiochemical properties using ^{H}NMR, Dynamic light scattering, Fluorescent Spectroscopic studies and TEM have clarified its drug carrying properties.

The critical aggregation concentration (CMC) is dependent on Degree of substitution (DS) of 5β Cholanic acid. It is lower than that of low molecular weight surfactant. Mean diameter of aggregate decreases with increase in DS of 5β Cholanic acid because of the compact inner core owing to enhanced hydrophobicity.[20] Thus, amphiphilic block copolymers and hydrophobically modified water soluble polymers forming micelle structure effectively carry drug with improved targeting with modified probes on surface. Theranostic, a combined diagnostic and therapy approach is recently applying HGC conjugates spontaneously self-assembled nanomaterials (CNP) for its application. Disease specific theranostic delivery systems use probes that can be used for drug delivery and contrast agents for imaging techniques like MRI.[31]

1.3.3 Factors influencing carrier properties

Interestingly high molecular weight chitosan (250kDa) has tumor targeting ability than low molecular weight derivatives (20kDa- 100kDa). It is found with higher molecular weight, blood circulation is prolonged with reduced time dependent excretion and thereby increasing tumor accumulation.[32] Molecular mass has some but minimal effect on viability, reduced toxicity and absence of hemolysis reported with shorter lengths.[26] Solubility depends on molecular mass and average distribution of acetyl groups along chitosan backbone, for example, uniform distribution of acetyl groups increased solubility by reducing crystallinity. Similarly stability and deformability is dependent majorly on Degree of substitution (DS) of 5β Cholanic acid, Increase in hydrophobicity made the nanoparticles more stable and rigid.[30] Chitosan aggregation is dependent on concentration, degree of acetylation, degree of polymerization, thus helping in fine tuning

structure property relationship in novel chitosan systems.[33] EPR process is also affected by various forms of surface thermodynamics.[26]

1.3.4 Promising carrier applications

Supramolecular micelles as drug delivery vehicles are generally unable to enter nucleus of non-dividing cells. HGC are potential carriers for nuclear targeting[34], tumor homing peptides like I4R binding interleukin-4 receptor[35] and, with photosynthetizer used in photodynamic therapy.[27] Self-assembled amphiphilic N(2,3,dihydroxypropyl)) chitosan-cholic acid (DHP-CS-CHO) proved to be a promising carrier of paclitaxel (PTX).[36] Nanoparticles containing homing peptides are expected to bind to tumor receptor and rapidly enter cancer cells through endocytosis.[35] Using orthogonal and synergetic mechanisms it could combine two or more drugs, encapsulating both chemotherapeutics and SiRNA to achieve maximum efficacy.[37]

1.4 Breast Cancer

In 2016, invasive breast cancer was diagnosed in about 246,660 women and 2,600 men. An additional 61,000 new cases of in situ breast cancer were diagnosed in women. [1]For adults aged younger than 50 years, cancer risk is greater for women (5.4%) than for men (3.4%) owing to high burden of breast, genital, and thyroid cancers in young women.[2] In underdeveloped countries, breast cancer remains prominent cause of cancer deaths among females. Although often referred to as a single disease, breast cancer is distinguished by up to 21 distinct histologic subtypes and at least 4 different molecular subtypes, which are associated with distinct risk factors and are biologically variable in presentation, response to treatment, and outcomes.[38] Reproductive and hormonal are leading risk factors for breast cancer cases, while long term menstrual history, recent use of contraceptives and menopausal hormone therapy are other considerations[3].

1.4.1 Breast cancer microcalcifications

Microcalcifications are tiny specks of mineral deposits (calcium) that can be scattered throughout the mammary gland, or occur in clusters.[39] Microcalcifications are most common abnormalities detected by mammography for breast cancer with high attenuation of X-rays over low attenuating breast tissue, present in about 30% of all malignant breast lesions, in over half of the malignant infra clinical breast lesions, and lead to depict 85 to 95% of all cases of ductal carcinoma in situ.[40] For these reasons a calcified region is considered a target for drug delivery aiming to kill cancer cells. Detection of these calcifications is limited by sensitivity and specificity of mammography.

1.4.2 Microcalcifications as target

In recent years bone seeking probes have been developed for Optical imaging and magnetic resonance imaging. Research has been carried out using these probes as a targeting agent for drug carrying vehicles. These probes are used to target high bone affinity. The compounds exhibiting strong affinity for bone tissues include heavy metals, polymalonic acid and most importantly geminal bisphosphonates, which are most utilized for this purpose[41].

Nanoparticles for contrast enhanced radiographic detection using breast calcification models that allow precise control over levels of Hydroxyapatite (HA) have been studied. Ex vivo models that closely mimic heterogeneity of breast cancer tissues studies state higher attenuation of other structures in breasts like fibrous tissue, ducts and blood vessels when compared to its surrounding tissues. Nanoparticles that provided greater X-ray attenuation, improved vascular retention, surface functionalities like colloidal stability and target delivery with the application of antibodies and peptides and non-cytotoxic behavior could help overcome this hurdle. Tumor

specific biomarkers are used for targeting the abnormalities. Bisphosphonate along with colloidal stability in physiological media has higher affinity to HA, which is also the mineral component of breast microcalcifications associated with malignant lesions.[42]

1.5 Bisphosphonates

Bisphosphonates (BPs) were introduced 45 years ago as anti-osteoporotic drug[43], known to inhibit bone resorption, and thus are being used as a treatment for osteoporosis.[44] Bisphosphonates are mainly used for inhibiting bone resorption caused by various factors but mostly due to aging. Bisphosphonates have strong interaction with Hydroxyapatite (HA), whose calcium ions provide bone- targeting property. Bisphosphonates that are used in treating bone disorders accumulate in areas of high bone metabolic activity utilized as bone-targeting groups[43]. They find application as probes for drug molecules, imaging agents for SPECT or Planar Scintigraphy, proteins and polymers and pain palliation treatments.[45] Aminobisphosphonates present a functionality that can be easily used for conjugation as they readily interact with other molecules, such as peptides, proteins, and ligands for protein recognition.[44] From the previous studies, maximum absorption capacity of bisphosphonates depends on size and electrostatic repulsion between negatively charged bisphosphonate groups. In this study, Amino bisphosphonates conjugated to biotin, a model linker for protein that can be attached to bone was investigated for its interaction with HA after biotinylation.

Major hindrances for imaging agent delivery include reticuloendothelial system (RES) and short circulation time. Bisphosphonate conjugated with Poly ethylene glycol polymer providing strong stable binding to surface of ultra-small superparamagnetic oxide (SPIO) nanomaterials, successfully providing platform for in vivo imaging SPIO for its MRI properties and low

cytotoxicity, yet the sudden break of BP-Iron bond contradicts slow rate of bisphosphonate release and in vitro stability.[46]

Bone targeting of therapeutic agents as it is engineered for bone affinity is done by incorporating a ligand. Bisphosphonate decorated lipid nanoparticles were able to entrap bone morphogenic proteins in a bioactive form and could deliver bioactive factors locally in mineralized scaffolds for bone tissue engineering.[47]

1.5.1 Alendronate

Alendronate is a clinically-approved BP that binds avidly to hydroxyapatite, the main component of bone mineral. Furthermore, provides an amino group conveniently separated from the BP group by a spacer, allowing facile one-step conjugation.[45]

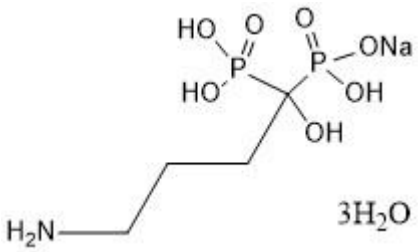

Figure 3. Alendronate chemical structure (drawn using Chemdraw).

Alendronate is a suitable candidate for its application as biomarker for our nanoparticles for high skeletal uptake and retention, binding rate greater than 80%, and stability after incubation with human plasma for 18 hours with negligible binding to serum proteins. Biodistribution studies to quantify uptake using HA, traces of bone and soft tissue organs prove alendronate is the most potent bisphosphonate for conjugation to nanoparticles.[45] Previous studies on dopamine self-polymerization on the poly(lactic-co-glycolic acid) (PLGA) particle surface and alendronate

conjugation and its direct binding to hydroxyapatite (HA) that could mimic calcified spots and HA porous scaffolds mimicking calcified tissues[48], and conjugations with functionalized gold nanoparticles[42], radiolabeled iron oxide materials[46], superparamagnetic iron oxide nanoparticles[49]. Insolubility of alendronate in organic solvents, complicating conjugation and high alkalinity of its amino group (pKa 12.7) inhibiting nucleophilic attack by alendronate using standard organic bases are major obstacles encountered during the development of alendronate conjugates.[45]

Previously, distearoylphosphoethanolamine-polyethylene glycol with 2-(3-mercaptopropylsulfanyl)-ethyl-1,1-bisphosphonic acid (thiolBP) was synthesized and incorporated into micelles and liposomes to create mineral-binding nanocarriers for therapeutic agents.[47] Nanoparticles that suffered poor loading and release, shortage of functional groups, difficulties to achieve active and passive targeting functionalities like PLGA (Poly (lactide-co-glycolide)) because of major ester groups with low reactivity with other functional groups. Chitosan modifies PLGA nanoparticles with versatile surface improved drug delivery.

1.6 Avidin-Biotin interactions

Molecular linkages within cellular interfaces arise largely from weak noncovalent interactions.[50] The avidin-biotin complex is known to be the strongest non-covalent interaction (Kd = 10-15M) among ligand and protein. Biotin is a vitamin, present in small traces in all living cells, critical for cell growth and Avidin is a biotin-binding protein that functions as antibiotic in the eggs.[51] The biotin-binding proteins avidin (from egg white) occupy a place of honor in many fields.[52]

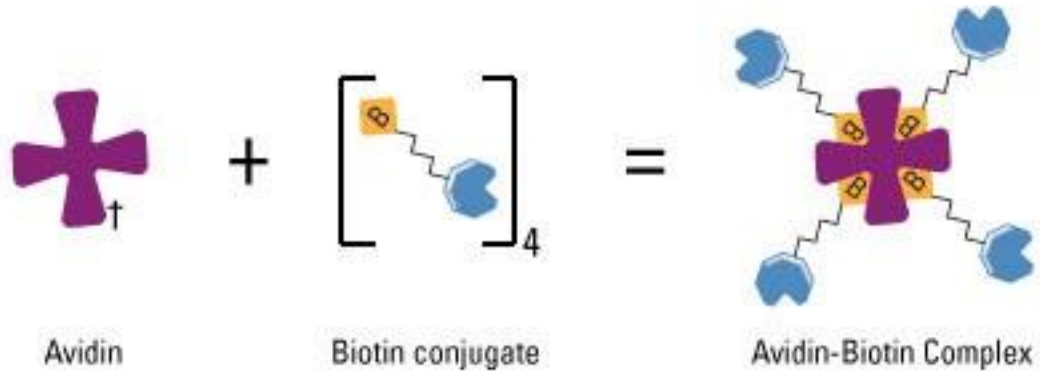

Figure 4. Biotin avidin interaction schematic[51]

Avidin–biotin complexation, considered an attractive strategy for the preparation of tumor targeted complexes and a widely-accepted approach in diagnostic applications. Nanoparticles were biotinylated and complexed to avidin equipped with multiple targeting ligands. Commonly, such strategies employ biotinylated tumor-specific antibodies and a therapeutic or diagnostic cargo coupled to avidin.[53] For instance biotinylated TRAIL interacted with RGD-equipped avidin and this complex was able to bind to the tumor maker αvβ3 integrins and effectively kill cancer cells.

Avidin, can bind up to four biotin molecules, as shown in the diagram below, making this an ideal interaction for purification and detection.[51]Physically, biotin-binding site is located adjacent to one end of the avidin barrel. It contains an array of polar and aromatic residues, all of which are involved in the tight binding. The binding site residues appear to be exquisitely positioned to provide a precise fit to biotin.[52]

The length of spacer arm of a biotinylation reagent influences its ability to bind to avidin. An elongated spacer arm improves availability of biotin for binding to avidin. Chemical groups between biotin and the functional side chain could modify the spacer arm length, as Sulfo-NHS-

LC-Biotin, which is water-soluble for ease of use and Ideal labeling reagent for monoclonal and polyclonal antibodies.[54]

In the current study we therefore pursue a chemical approach, employing an avidin– biotin approach as the bond formation between biotin and avidin is very rapid, and once formed, is unaffected by extremes of pH, temperature, organic solvents and other denaturing agents.[51]

1.6.1 HABA assay

HABA (4'-hydroxyazobenzene-2-carboxylic acid), a reagent that estimates biotinylation levels. HABA-avidin complex has absorption peak at the 500nm wavelength. Biotinylated molecule is added to HABA/avidin premix, the absorbance drop is proportional with the amount of biotin. Thus, the biotinylation level of the sample can be assessed with absorbance.

1.7 Fluorescence labelling

Using of fluorescence-derived contrast to quantify, distinguish and investigating nanoparticles, drugs, cells and tissue is considered a universal strategy Cyanine, fluorescein isothiocyanate (FITC), Alexa Fluor, Dylight Fluor, rhodamine, 4',6-diamidino-2-phenylindole (DAPI), etc., are commonly used fluorescent probes. Fluorescence microscopy provides a comprehensive tool for investigating many of these aspects of drug delivery[55].

1.8 Particle characterization

Dynamic light scattering (DLS) was the technique used for determining the size distribution of small particle suspension or polymers in solution. DLS can also be used to probe

complicated behaviors of complex polymer solutions. Commercial DLS instruments combine particle size measurements and zeta potential analyzers for characterizing a wide array of materials.

In field of nanocharacterization, TEM accomplishes Imaging, measuring, modeling, and manipulating.[56] The transmission electron microscope (TEM) operates on the same basic principles as the light microscope but uses electrons instead of light capable of seeing objects to the order of a few angstroms (10^{-10} m).

Absorption peaks of infrared spectrum represent fingerprints of studied sample each corresponding to frequencies of vibrations between the bonds of the atoms making up the material. Each different material is a distinctive arrangement of atoms, no two compounds construct the exact same IR spectrum. Therefore, IR spectroscopy results in a qualitative analysis of different kinds of materials. Fourier Transform Infrared (FT-IR) spectrometry was established to overcome the boundaries met by ancestor instruments like slow scanning process. FTIR can measure all the infrared frequencies simultaneously.[57]

Chapter 2: Objective

Aminomethylene bisphosphonic acid presents amine functionality that can be easily attached to a biomolecule. This property supports our hypothesis that Bisphosphonate (BP) probe can be attached to our HGC nanoparticle using Avidin biotin interaction for targeting microcalcification that is one of the pathological signs of breast cancer. The main objective of this study is conjugation of Alendronate, a bisphosphonate drug with Hydrophobically modified glycol chitosan micelles (HGC), a proven candidate for its high biocompatibility, biodegradability, functionalization and rapid uptake by both osteosarcoma and breast cancer cells and examine the physicochemical properties and targeting efficiency of these nanoparticles modified for target-selectivity. Subsequent theranostic potentials as imaging probes for early breast cancer detections and anticancer drug delivery system are studied.

To test our hypothesis, we: (1) prepared HGC-based nanoparticles and conjugated alendronate via the biotin-avidin- biotin binding with Cy3 fluorescent marker, (2) characterized the physiochemical properties of nanoparticles and (3) studied and compared their binding affinity in a Hydroxyapatite model.

Aim 1: Alendronate sodium was biotinylated at the amine group with Sulfo-NHS-LC-biotin. Sulfo-NHS-LC-biotin was added to the amine (-NH2) groups on GC (glycol chitosan) to prepare the Biotinylated Glycol Citosan (BGC). BGC was then avidinylated via the avidin-biotin interaction. BGC-A was hydrophobically modified by adding 5ß cholanic acid (BHGC-A). Micelles were surface modified with biotinylated alendronate and labeled with fluorescent dye Cyanine 3 to quantify the binding of nanoparticles to HA.

Aim 2: The nanoparticles prepared with and without alendronate surface functionalization were characterized using dynamic light scattering technique for size measurements, zeta potential analyzer for surface charge distribution and FTIR (Fourier transform infrared spectroscopy) for analyzing the chemistry of synthesized nanoparticle.

Aim 3: Binding affinity of these nanoparticles at various time points was studied and compared by incubating three different concentration of hydroxyapatite in nanoparticle suspension at a concentration of 50µg/mL for up to 24 hours by measuring Cy3 fluorescence intensity of supernatant of incubated nanoparticle suspension after centrifuging and pellet was studied for the binding chemistry using FTIR analysis.

Chapter 3: Materials and Methods

3.1 Materials

Glycol chitosan (250kDa molecular weight, degree of deacetylation ≥ 60% (titration)), 5β-cholanic acid, Alendronate Sodium Trihydrate, N-hydroxysuccinimide sodium salt, Triton X-100 solution, 37% in water formaldehyde solution, 1-Ethyl-3- (3-dimethylaminopropyl) carbodiimide hydrochloride (EDC), Hydroxyapatite and 4-(Dimethylamino)pyridine (DMAP) were purchased from Sigma-Aldrich (St. Louis, MO). HABA (4'-hydroxyazobenzene-2-carboxylic acid)/avidin assay, Sulfo-NHS-LC-Biotin, avidin from egg white and Alexa Fluor®546 phalloidin were purchased from Thermo Fisher Scientific(Rockford, IL). Monoreactive hydroxysuccinimide Cyanine 5.5 (Cy5.5 NHS ester) was purchased from Lumiprobe (Hallandale Beach, FL). Anhydrous dimethyl sulfoxide (DMSO) was purchased from EMD Chemicals (Darmstadt, Germany). The 4T1 murine mammary carcinoma cell line was purchased from the American Type Culture Collection (Manassas, VA). Serum-free, phenol red-free Dulbecco's Modified Eagle Media (DMEM) was obtained from Gibco (Carlsbad, CA).

3.2 Nanoparticle Synthesis

Hydrophobically modified glycol chitosan (HGC) nanoparticles were synthesized with biotinylation, avidinylation and hydrophobic modifications. Further the nanoparticles were functionalized with alendronate sodium using biotin-avidin interaction. The detailed synthesis procedures for HGC synthesis are described in Section 3.2.1 and alendronate conjugation in 3.2.2.

3.2.1 Synthesis of HGC nanoparticles

The synthesis of HGC nanoparticles flow diagram is shown in Figure 5. Sulfo-NHS-LC-biotin was added to the amine groups on glycol chitosan synthesizing "N-type" nanoparticles as Sulfo-NHS-LC-biotin was conjugated to the $-NH_2$ groups[58] followed by avidinyation and micellization with hydrophobic modification with 5ß cholanic acid.

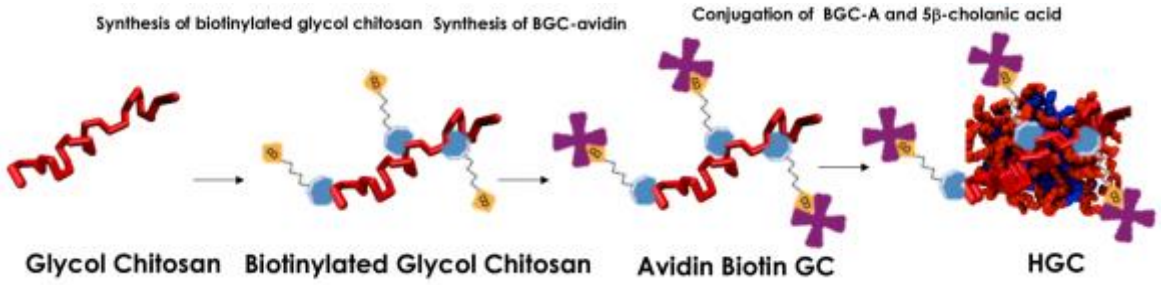

Figure 5. Synthesis of HGC nanoparticles flow diagram (drawn using MS powerpoint)

3.2.1.1 Biotinylation of Glycol Chitosan

The biotinylated glycol chitosan (BGC) was synthesized by reacting NHS ester on Sulfo-NHS-LC-biotin with amine on glycol chitosan. Three hundred milligrams (1.2 µmol) of glycol chitosan (MW 250 kDa) were dissolved into 36 mL of HPLC water in a 250mL beaker and stirred until the solution was clear. Ten milligrams (0.018 mmol) of SulfoNHS-LC- biotin (MW 556.59

Da) were added dropwise to 250 mL beaker containing glycol chitosan solution making a 1:15 GC to biotin molar ratio. Mixture was stirred for 3 hours using a magnetic stir bar after which the solution was loaded to a 10k MWCO dialysis cassettes using a syringe (20mL) and needle (20Gx1 0.9mmx25mm). The mixture was dialyzed against 1600 mL HPLC water for two days changing media twice per day. After dialysis, the retentate was lyophilized for three days and ground into a fine powder and stored at -4ºC.

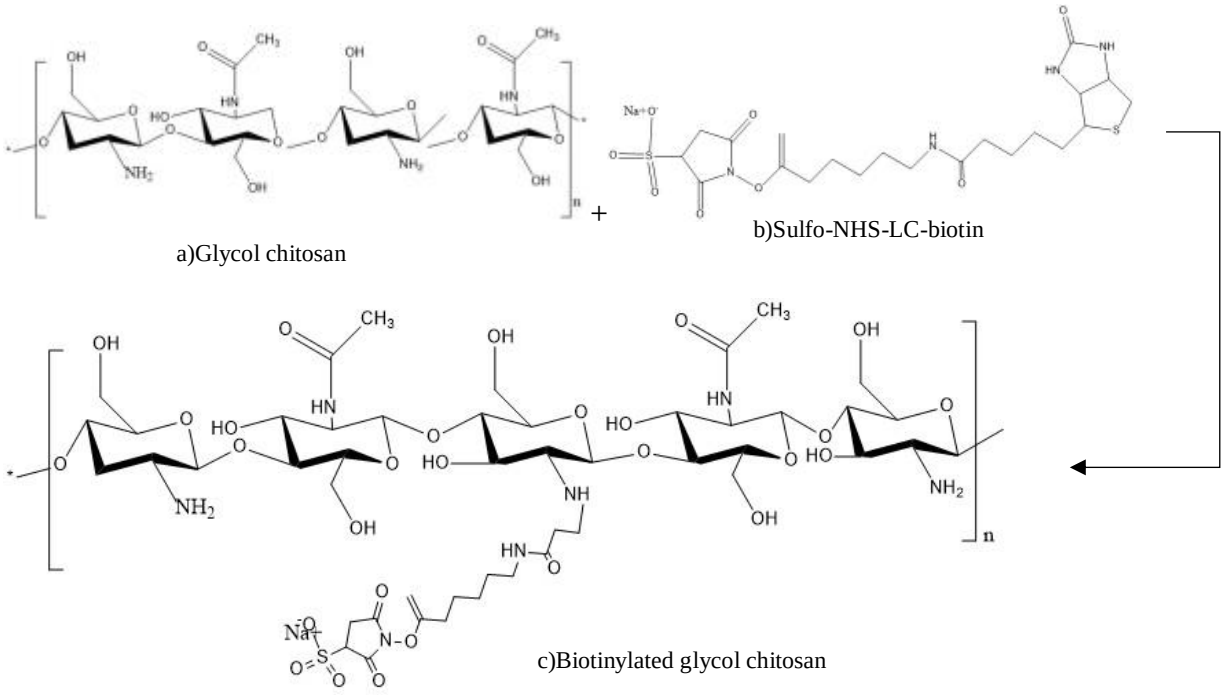

Figure 6. Chemical Synthesis of Biotinylation of glycol chitosan- a) Glycol chitosan was reacted with b) Sulfo-NHS-LC Biotin to give c) Biotinylated glycol chitosan (structures drawn using Chemdraw)

3.2.1.2 Biotin Quantification – Biotinylation Level

Biotinylation level was the measure of amount of biotin conjugated to one polymer. Biotin quantification kit helps in measuring the biotinylation level using the absorbance after reaction with HABA avidin premix, a control biotinylated HRP (Horseradish Peroxidase) was used to compare and evaluate correctness the assay.

3.2.1.3 Biotin Quantification HABA assay

The biotinylation level of BGC was determined with HABA assay. Biotinylated glycol chitosan (BGC) was dissolved into PBS at 1mg/mL concentration. One hundred microliters of HPLC water was added to one microtube containing the HABA/Avidin Premix from Pierce Biotin Quantitation Kit. Seven wells of a 96-wells microplate each added with 160 µL of 1xPBS and 20 µL of the HABA/Avidin Premix solution. Mixture was mixed with an orbital shaker for 2 minutes before measuring the absorbance at 500 nm with the microplate reader. In each well 20µL of prepared biotinylated glycol chitosan solution (1mg/mL) was added and incubated at room temperature for 3mins. The solution was mixed again with an orbital shaker for 2 minutes before measuring the absorbance at 500nm.

$$mmol\ BGC\ per\ ml = \frac{BGC\ Concentration\ (\frac{mg}{mL})}{Molecular\ weight\ of\ BGC\ (\frac{mg}{mmol})} \quad (1)$$

$$mmol\ of\ biotin\ per\ mmol\ of\ BGC = \frac{mmol\ biotin}{mmol\ BGC\ per\ mL * mL\ solution} \quad (2)$$

$$Biotinylation\ efficiency = \frac{mmol\ of\ biotin\ per\ mmol\ of\ BGC}{molar\ ratio\ of\ biotin\ added\ to\ BGC} \quad (3)$$

The amount of biotin in biotinylated chitosan was calculated according to the manufacture's instruction. Biotinylated HRP given with the quantification kit was used as the positive control. (biotinylated level was 1 for HRP as per product label). The biotinylation efficiency was calculated using equation 3.

3.2.1.4 Avidinylation of BGC

Avidin was attached to BGC through the avidin-biotin binding. Two hundred milligrams of BGC was added to 30 mL of water in a 100mL beaker and were dissolved until clear. From the biotinylation level obtained from HABA assay (12.67) the amount of avidin was calculated with an avidin to biotin molar ratio of 1:8 as each avidin molecule can accommodate maximum of four biotin molecules. 81.5 mg of avidin were added to 10 mL of water in a 15mL falcon tube, shaken and vortexed to dissolve. The avidin solution (81.5 mg/1.235 µmol) to BGC solution (8:1 mol/mol biotin: avidin) were added dropwise and let stir for 2 hours. BGC solution was diluted to 48 mL with water by adding 14mL HPLC water and loaded to four 100 k MWCO Amicon tubes (Amicon Ultra-15 Centrifugal Filter Unit with Ultracel-100) as 12 mL each tube. The centrifugal filter units were centrifuged at 5,000xg for 20 min at room temperature with the fixed angle rotor from CME laboratory at room temperature. The concentrated extract BGC solution sample was collected in a 50mL falcon tube, freeze-dried for three days and ground into a fine powder and stored at -4ºC.

3.2.1.5 Hydrophobic modification of NPs with 5ß cholanic acid

Hydrophobically modified glycol chitosan (HGC) was synthesized via the reaction between the 5ßcholanic acid the hydrophobic component that forms the micelle core and the biotinylated glycol chitosan in the presence of 1-Ethyl-3- (3-dimethylaminopropyl) carbodiimide hydrochloride (EDC) and N-hydroxysuccinimide. The synthesis of Glycol Chitosan Nanoparticle

was conducted in a chemical Fume hood due to the usage of methanol as a major solvent in the process. Two hundred milligrams of BGC-A were dissolved into 36mL of HPLC water in a 100mL beaker. In another beaker 40mg of 5ßcholanic acid was dissolved into 17mL of methanol and stirred until clear. To the beaker containing 5ßcholanic acid solution 32mg of EDC and 19mg of NHS was added. 5ßcholanic acid solution is transferred to the BGC-A solution and mixed over night at room temperature.

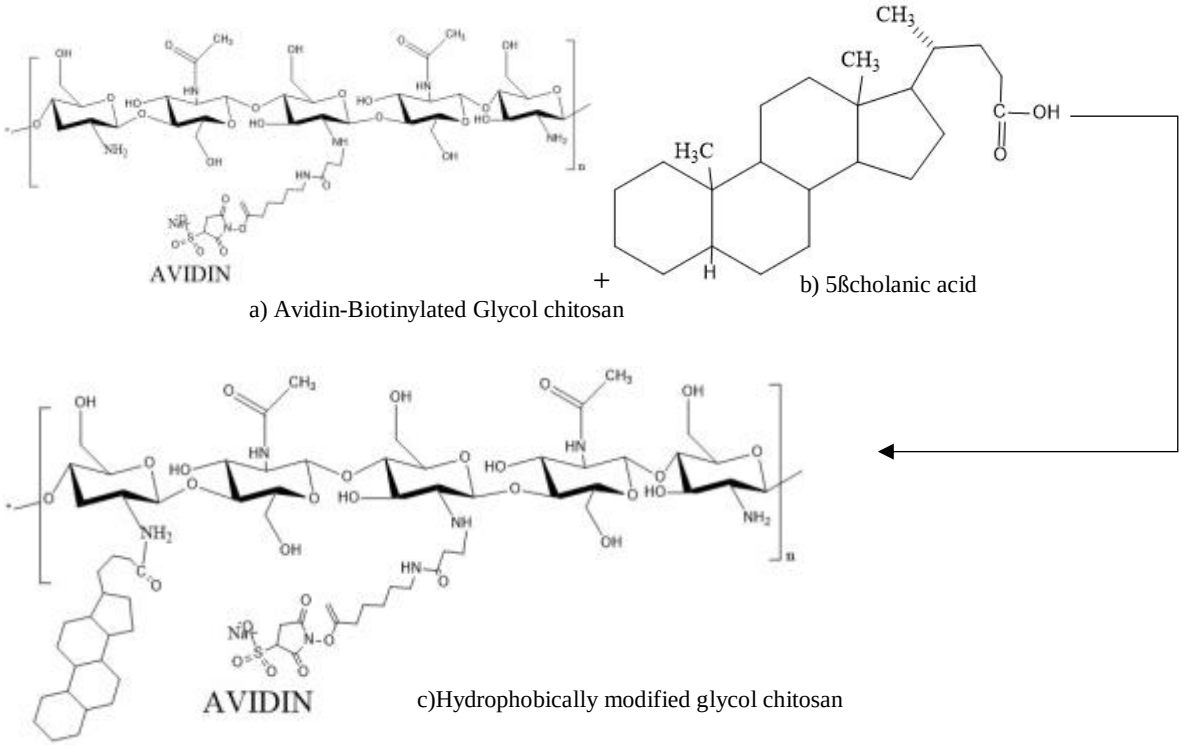

Figure 7. Chemical Synthesis of Hydrophobically modified Avidin-Biotinylated glycol chitosan a) Avidin-Biotinylated Glycol chitosan was conjugated with b) 5ßcholanic acid to yield c) Hydrophobically modified glycol chitosan (structures drawn using Chemdraw)

Sample was loaded into two 30mL 10K MWCO dialysis cassettes using a syringe (20mL) and needle (20Gx1 0.9mmx25mm) and dialyzed against methanol/water (1:4) mixture for one day, changing the media twice, while covering it with foil paper to avoid dust and evaporation. The

solution was dialyzed against water for second day. The sample was unloaded to three 50mL falcon tubes. After centrifuging for 30mins it was frozen at -80ºC and lyophilized and ground into a fine powder and stored at -4ºC.

3.2.1.6 Cy3 labeling of nanoparticles

Thirty milligrams of BHGC-A were dissolved into 20 mL DMSO in a 100mL beaker and stirred until it was dissolved. Sixty microlitres of Cy3 in DMSO stock solution at 5mg/mL concentration was added to the BHGC-A solution dropwise. After stirring for 6 hours, in the dark, the reaction mixture was loaded into 10K MWCO dialysis cassettes and dialyzed against 1600 mL HPLC water in a 2000 mL beaker for two days. The medium was changed every two hours for the first 4 hours of each day.

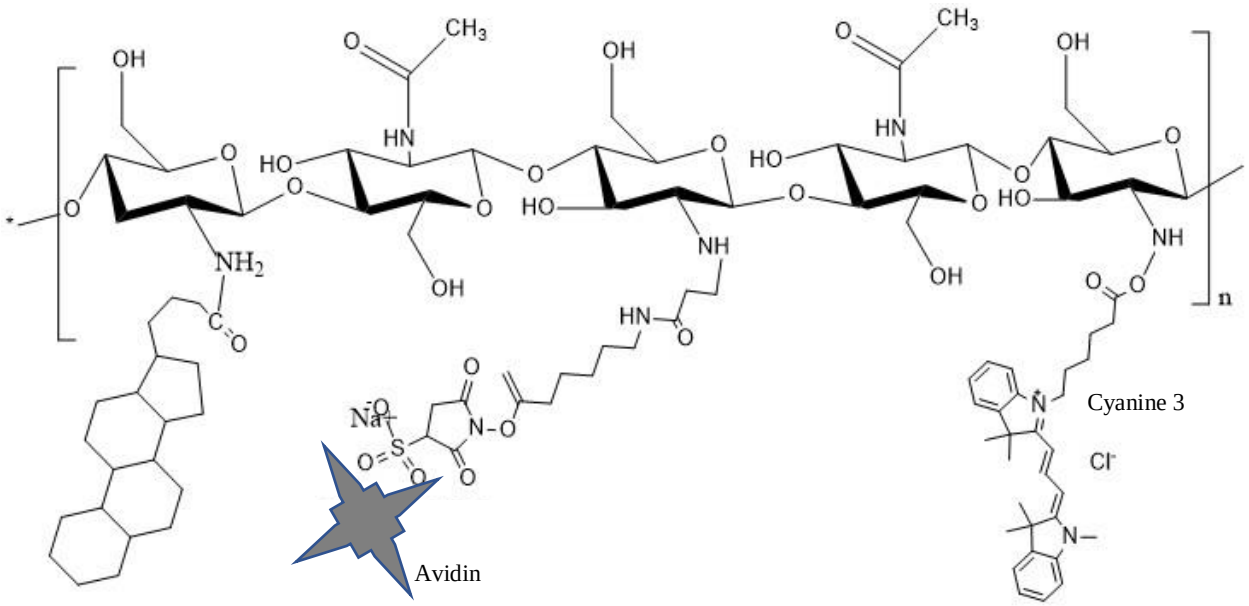

Figure 8. Cyanine 3 was attached to the amine group of chitosan to Cy3 labelled BHGCA nanoparticles (Structures drawn using Chemdraw)

The mixture was unloaded to 50 mL falcon tubes, centrifuged to allow phase separation and frozen at -80ºC overnight. The frozen mixture was lyophilized for 3 days after which it was ground and stored in -4ºC freezer and ground into a fine powder and stored at -4ºC for further use.

3.2.2 Preparation of alendronate functionalized nanoparticles

The nanoparticles prepared as mentioned in section 3.2.1 were functionalized with alendronate sodium using biotin-avidin interaction. Biotin from biotinylated alendronate was conjugated with avidin from Hydrophobically modified biotinylated avidinlyated glycol chitosan nanomicelles forming a strong avidin-biotin bond.

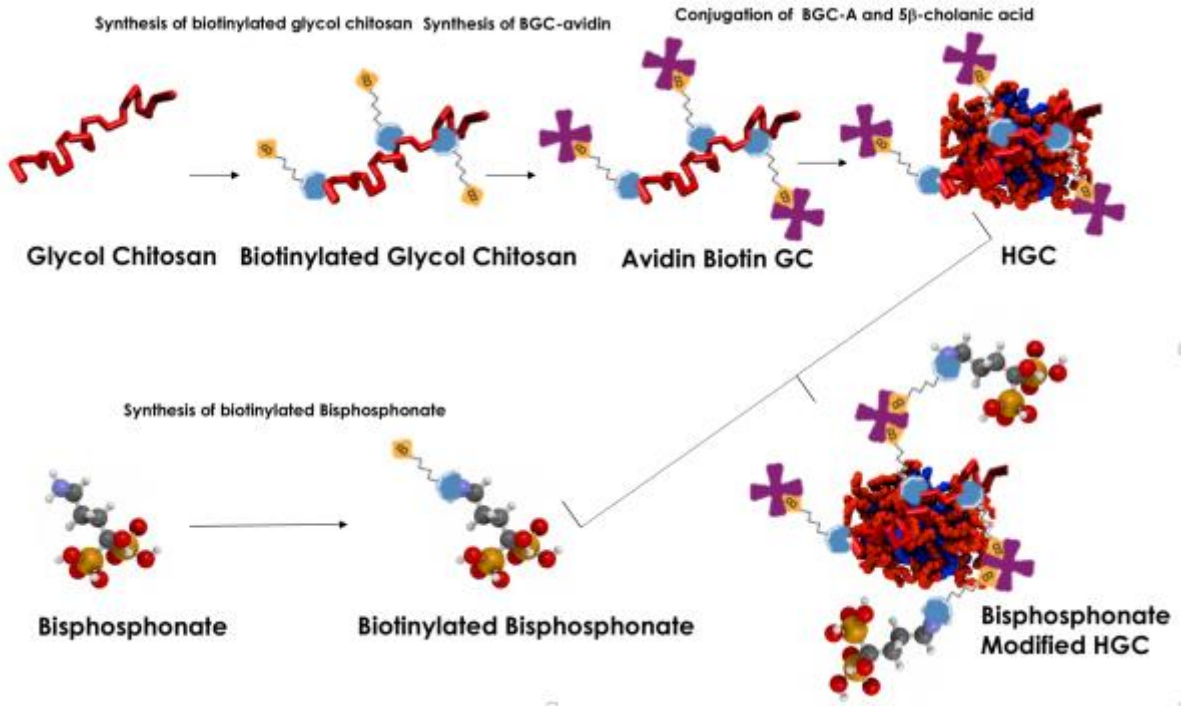

Figure 9. Experimental design for making BHGCA-BALN nanoparticle (Drawn using MS Powerpoint)

3.2.2.1 Biotinylation of Alendronate

Synthesis of biotinylated Alendronate with 1:1 biotinylation level, reaction was carried out as NHS ester on Sulfo-NHS-LC-biotin with amine on alendronate sodium. Twenty-five milligrams of Alendronate Sodium were dissolved into 20mL of HPLC water in a 250mL beaker and stirred until clear. Eighty-six milligrams of Sulfo-NHS-LC- biotin was dissolved in 10 mL of HPLC water in a 15mL falcon tube and used immediately by Transfer Sulfo-NHS-LC- biotin solution dropwise into the 250mL beaker with alendronate solution. After stirring for 3 hours the solution was freeze dried for three days, ground and stored in -4C° freezer for further use.

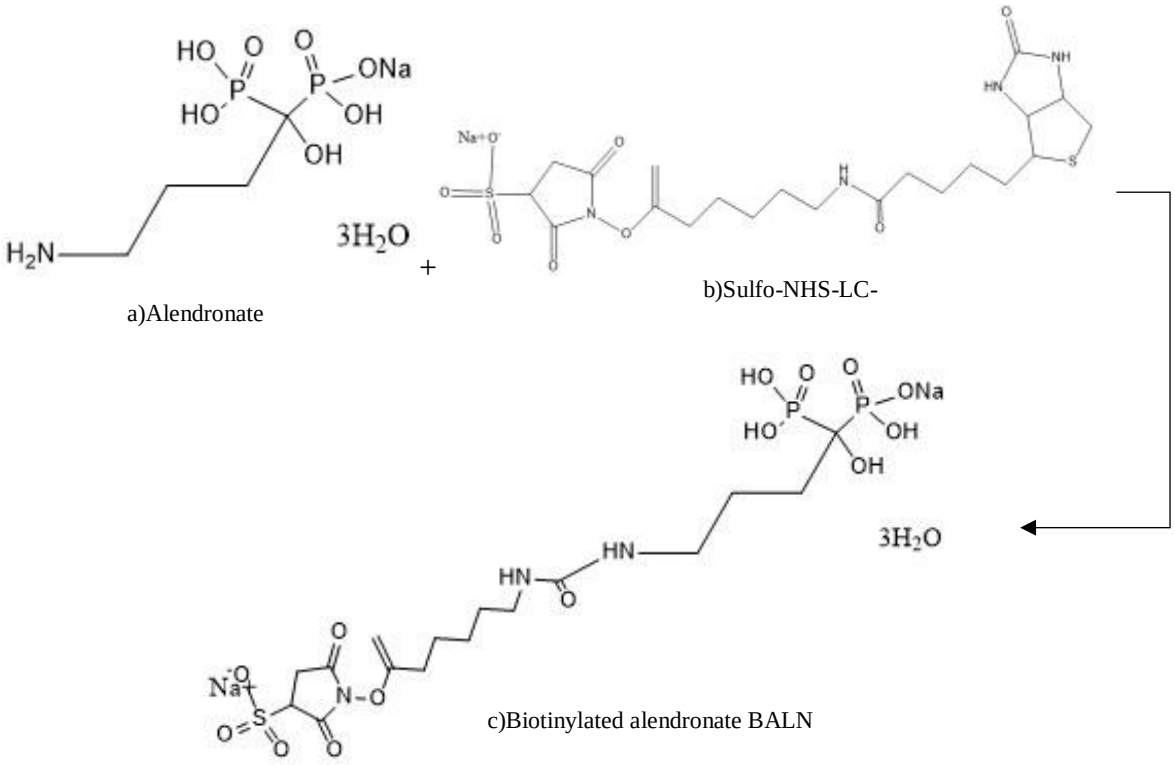

Figure 10. Chemical Synthesis of Biotinylated alendronate- a) Alendronate was reacted with b) Sulfo-NHS-LC Biotin to yield c)Biotinylated alendronate BALN (structures drawn using Chemdraw)

3.2.2.2 Alendronate conjugation and Cy3 labeling of nanoparticles

The Cy3 labeling of BHGC-A nanoparticles was obtained by the same strategy as described in Section 3.2.1.5. After adding Cy3 and stirring for 6 hours, in the dark, 1.6 mL (1.560 mg) of biotinylated ALN from a stock solution in HPLC water at 1 mg/ mL concentration was added to the mixture. Followed by stirring for 2 hours, in the dark, the reaction mixture was dialyzed, lyophilize and final ground as explained in 3.2.1.5. The nanoparticle powder was stored in -4ºC freezer for further use.

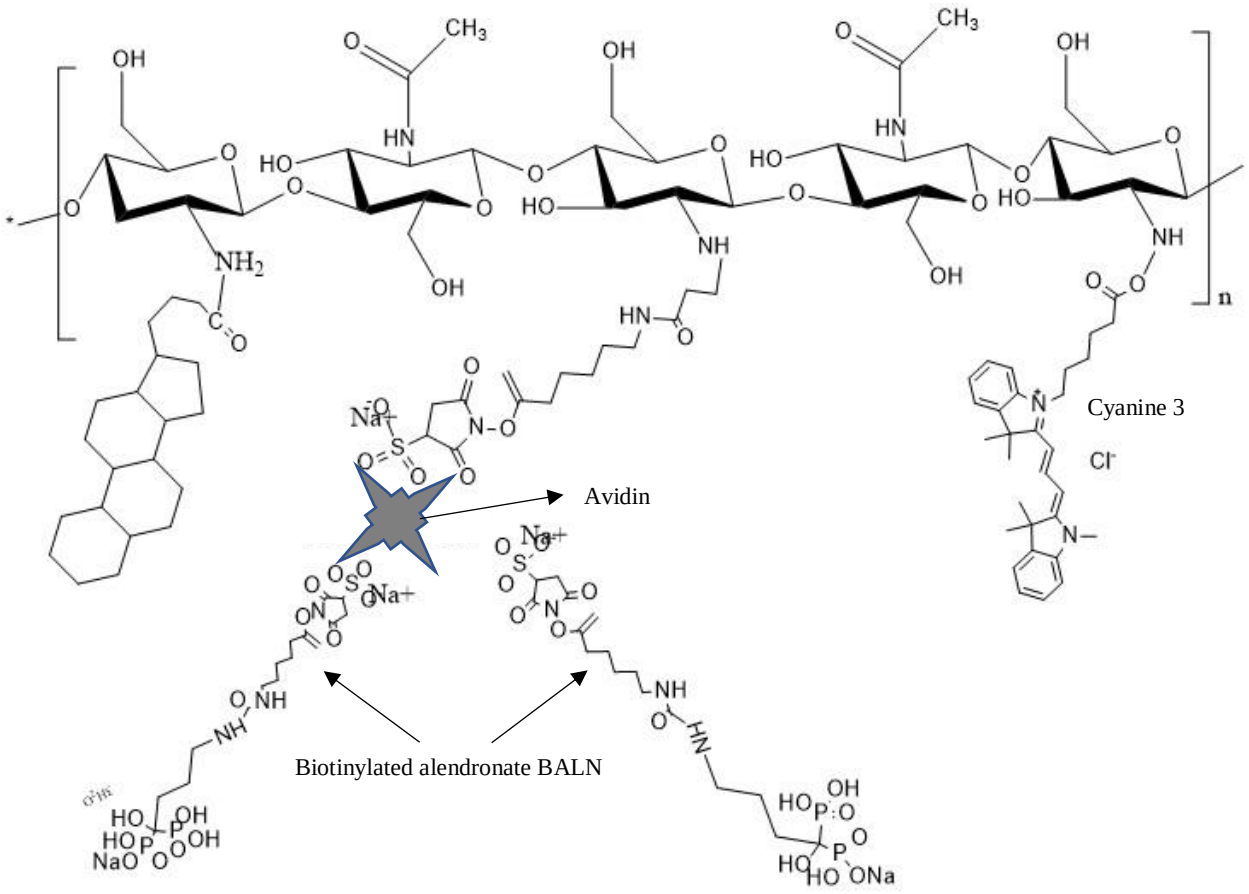

Figure 11. Biotinylated alendronate was conjugated and Cyanine 3 was attached to the amine group of chitosan to Cy3 labelled BHGCA nanoparticles (Structures drawn using Chemdraw)

3.2.2.3 Biotin quenching of Cy3 BHGCA nanoparticle

To study the binding kinetics further and avidin's role in sticking the nanoparticles to HA crystals, the free avidin spots were quenched by adding 4 mg of Sulfo NHS biotin to 40 mg of Cy3 BHGCA to make Biotinylated Cy3 BHGCA (BHGCAB) in HPLC water. The mixture was dialyzed using 10k MWCO cassettes and freeze-dried as mentioned in 3.2.1.5 and stored in -4˚C freezer.

3.2.3 Preparation of nanoparticle suspension

To treat the nanoparticle to cells or material characterization, suspending it in a medium was an essential step. An HGC suspension at 1mg/mL concentration was required, so 8mg of HGC was weighed and added to 8mL of HPLC water. The solution was vortexed and bath sonicated for 10 minutes and probe sonicated for about 10 minutes on ice to obtain a homogenous suspension. Then the sonicated solution was carefully filtered with 0.8µm and 0.2µm syringe filters to avoid the undissolved chunks of powder and obtain a HGC nanoparticle suspension. The suspension was stored at 4ºC for further use.

3.3 Particle size and zeta potential measurements

In the experimental process DLS instrument (Malvern – Zetasizer Nano ZS90) from Brookhaven National Laboratory was used for determining the size of our Cy3-BHGCA and Cy3-BHGCA-BALN nanoparticle sample. The synthesized nanoparticle suspension was prepared in HPLC water at concentration of 0.25mg/mL, in two 15mL sample holders. The device software from Brookhaven Instruments was installed in the computer connected to the DLS instrument. After installation, the software was started and DLS particle size measurement option from the list given was selected. Before the size measurement of the nanoparticle, the parameter and operating

condition was checked. The parameters could be altered by SOP (Standard Operating Protocol) option where we can provide information of various parameters including the solvent (in this case water). The sample was moved from sample holder to DLS cuvette using a pipette. The cuvette was inserted into the instrument and experiment was started. Three measurement values were iterated taking a few minutes to complete (2 min for each iteration). The data was obtained and saved for analysis. To measure the Zeta potential 1mL of sample was moved back into the sample holder and an electrode cap was inserted into the cuvette. The cuvette was put back into the instrument for measurement of zeta potential. The wire from the electrode was connected to the socket in the instrument. The operating conditions include 90º of scattering angle (it can be either front scattered or back scattered), Temperature of 25(room temperature) and number of repetitions as 3.

3.4 Binding affinity studies

Three different volumes of HA crystals (50mg, 100mg, 200mg) were added to a 12 mL of BHGCA-ALN and BHGCA NP suspension in HPLC water with concentration of 50 µg/mL. Suspensions were placed onto a test tube rotator (rock n heat) and allowed to incubate for 24 h. After the solutions were centrifuged for 2 min to separate HA crystals and bound NPs from NPs remaining in solution. At different time points, sample was collected to find the percentage binding, which was defined as the concentration of NPs remaining in the supernatant after binding, subtracted from the initial concentration of NPs in solution, and divided by the initial concentration of NPs. Binding of functionalized NPs to the surface of HA crystals was studied by FTIR after drying the collected HA crystals from pellets.

3.5 FTIR analysis

Fourier transform infrared spectroscopy (FTIR) technique was used to obtain an infrared spectrum of absorption data over a wide spectral range to understand the synthesis and binding chemistry for our studies.

3.5.1 Air-drying the sample for FTIR

The 200 mg pellet after the binding affinity experiment was utilized for FTIR. The sample was air-dried to avoid water peaks from the FTIR experiment. Pellet was spared on an aluminum foil using a spatula. The foil was placed inside a 10cm cell culture dish and lid is closed leaving a small opening for air. Setup is kept aside for 2 days. The sample after drying, in the form of fine powder was collected and moved to 2 mL eppendorf tube for further experimentation.

3.5.2 FTIR experimental setup

Liquid nitrogen was filled into the Thermo Scientific Nicolet iS50 FT-IR spectrometer machine, which acts as the cooling system. The Moisture should be avoided all time during the experiment thus a moisture indicator was checked for Green color that signifies dry experimental conditions. Air gauge was checked for 30 units in pressure gauge and 40 units in airflow meter for machine operating conditions. OMNIC Software was used for collecting and analysis of data. Number of scans was selected as 128 and resolution was set to 4. Before collecting FTIR data for each sample under study background air was measured using collect background option from the software and saved in a file, this saved air background was used to subtract each time we work with a sample. Later about 2 mg of sample was loaded on a sample mount placed over the crystal base and the knob was tightened. The FTIR date for respective sample was collected using collect sample option

from the OMNIC software. The sample mount, knob and crystal base were cleaned for the next sample and the process was repeated.

Chapter 4 Results

4.1 Nanoparticle synthesis

The nanoparticle synthesis involves several steps as explained in previous section. The commercially available glycol chitosan was in a fine power form and was readily soluble yielding a gel like clear solution after dissolved and added with biotin. The freeze-dried sample of GC when attempted ground to a fine powder resulted in ground powdery flakes, thus during avidinlynation, the BGC dissolution was slower and rigorous stirring was needed for obtaining a clear solution. While grinding biotinylated alendronate, Cy3-BHGCA nanoparticles and Cy3-BHGCA-BALN nanoparticles, finely powdered form was achieved.

4.1.1 Biotinylation efficiency

The targeted biotinylation molar polymer to biotin ratio was 1:15 optimized by previous studies. The biotinylation efficiency of biotinylated HGC (BHGC) was determined with HABA assay. BGC was dissolved in water in 15mL sample holder tube by vortexing for 10 minutes. A Corning 96 Flat Bottom Clear Polystyrene UV transparent plate was used to avoid absorbance due to the microplate. The biotinylation efficiency was determined by equation 3 from previous section and results are listed in Table 1. The average biotinylation efficiency was found to be 84.5% for first batch and 93.8% for second batch, which indicated that more than 80% of the biotin molecules was conjugated to the GC polymer.

Batch	HGC(mg)	Biotin(mg)	Molar ratio (GC:B)	Amount of Biotin per HGC	Biotinylation efficiency
1	300	10	1:15	12.676	84.5%
2	300	10	1:15	14.07	93.8%

Table 1. Biotinylation efficiency

4.1.2 Cy3 Labeling

To quantify the amount of nanoparticle in a solution to determine the binding efficiency etc. it is crucial for it to have a signature in terms of absorbance or fluorescence. The hydrophobically modified glycol chitosan nanoparticles do not have a fluorescence signature to it. The absorbance scan of alendronate did not show notable peaks of peak in solvents like HPLC water and DMSO at 1mg/mL and 0.1mg/mL concentration as shown in the Figure 12.

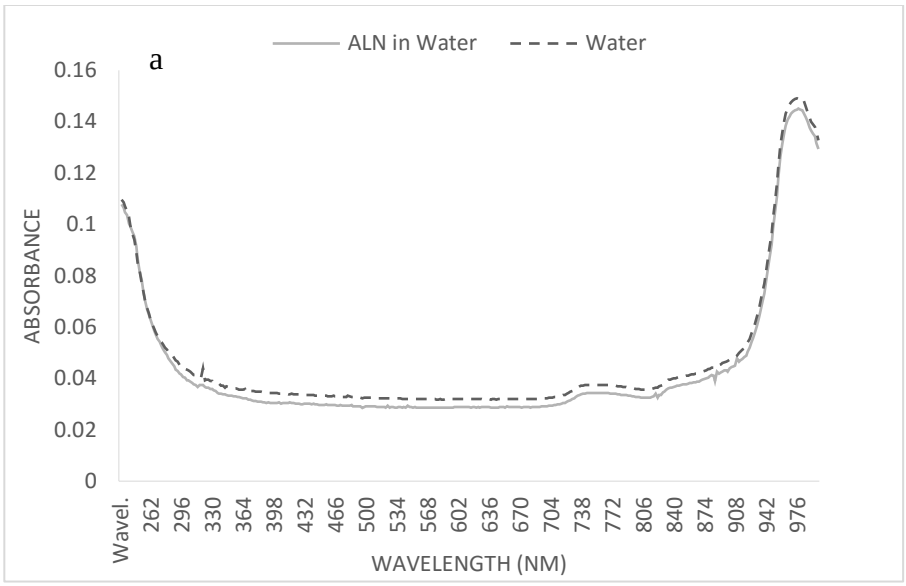

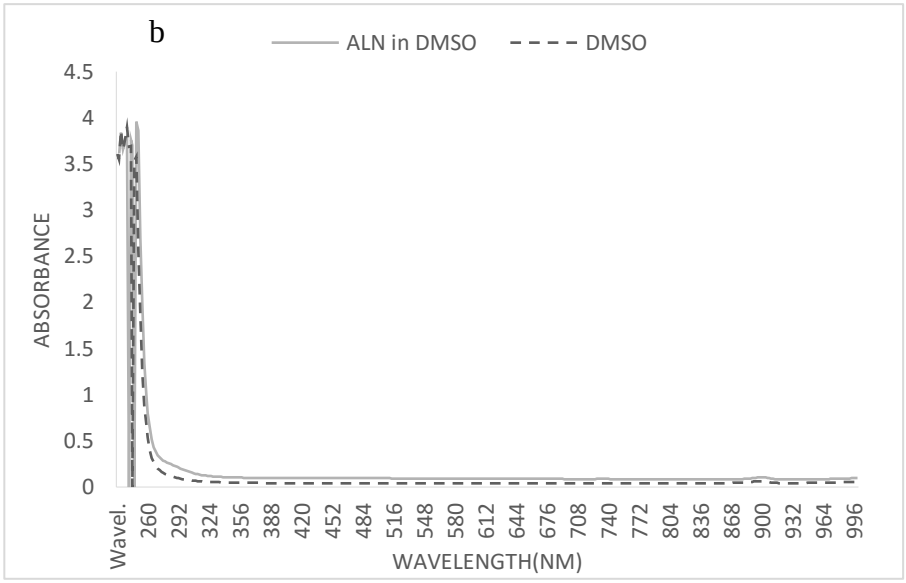

Figure 12. UV-Vis absorbance scan of a) ALN in HPLC water vs plain HPLC water, b) ALN in DMSO and plain DMSO

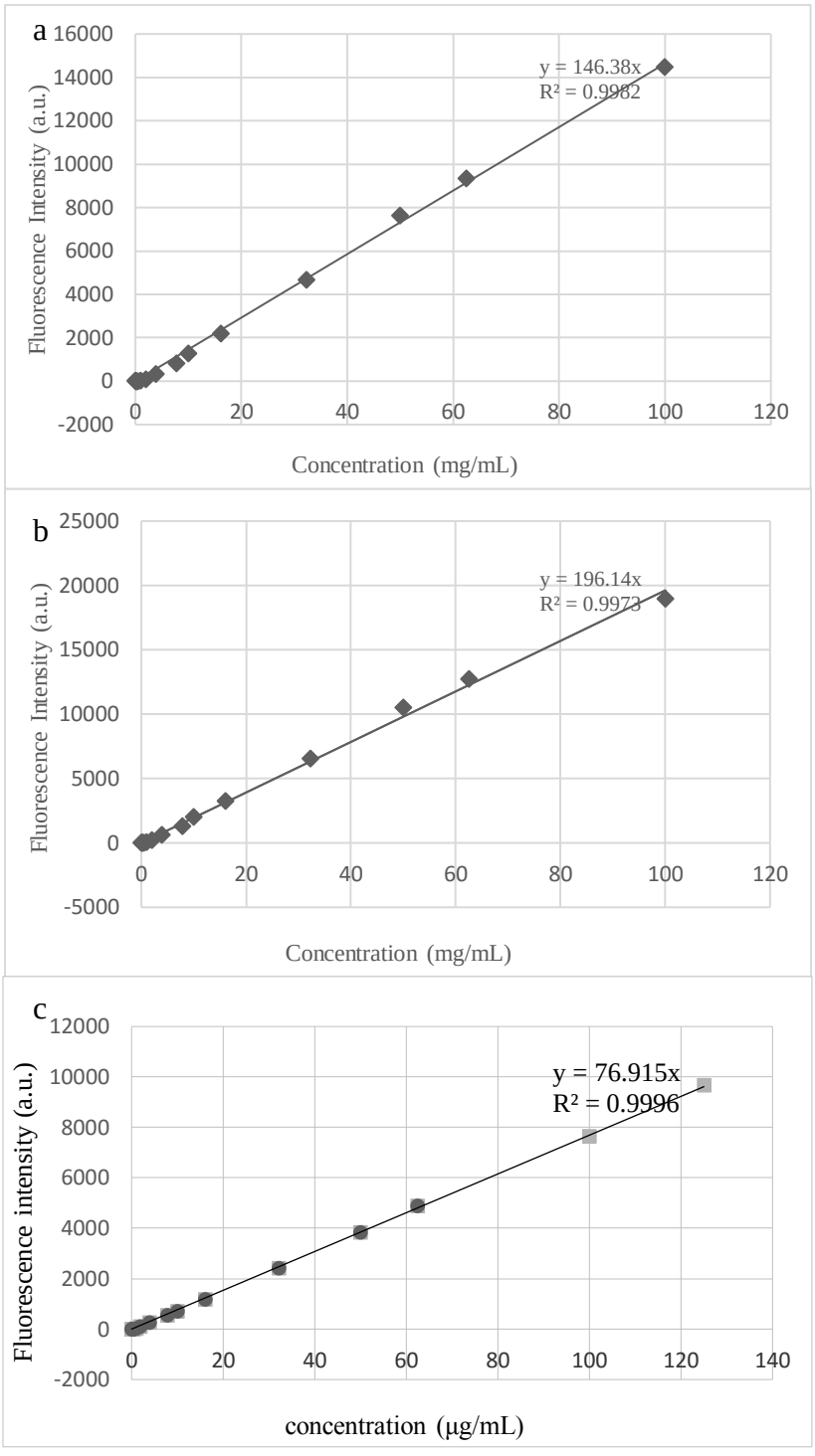

Figure 13. Standard concertation curve for a) Cy3-BHGCA-BALN b) Cy3-BHGCA c) Cy3 BHGCA Biotin prepared in water.

To study the nanoparticle for concentration and imaging it was conjugated with Cy3, a fluorescent agent. The standard fluorescent intensity curve was obtained by creating solutions with different concentration ranging from 0.06µg/mL to 100µg/mL and obtaining fluorescent intensity for each concentration and plotting a graph with obtained data as shown in the Figure 13. The trend line for the obtained plot was mapped to a linear equation and obtained R^2 values were very close to 1 (~0.997). The higher R^2 value is an indication of a respectable correspondence between actual and predicted values. The linear equation obtained from the graph was used for mapping fluorescent intensity to concentration in further experiments.

4.2 Size and zeta potential

Cy3 conjugated HGC Nanoparticle with and without alendronate functionalization was suspended in HPLC water using same step followed in previous section on preparation of nanoparticle suspension. The hydrodynamic diameter and zeta potential of both the nanoparticles suspended in water was measured with DLS and zeta potential at room temperature in three iterations. The average diameter was 254.0 ± 0.43 nm and 209.7 ± 1.0 nm for Cy3-BHGCA and Cy3-BHGCA-BALN nanoparticles respectively. The average surface charge was +26.9 ± 0.19 mV and +27.68 ± 0.20 mV for Cy3-BHGCA and Cy3-BHGCA-BALN nanoparticles respectively represented by the Table 2 as shown below. The effective diameter of alendronate conjugated nanoparticle was approximately 40nm less than the nanoparticle without alendronate attached to it. The surface charge remains similar in both the nanoparticles.

Chitosan nanoparticles	Size (nm)	Zeta Potential (mV)
Cy3 BHGCA NP	254.0 ± 0.43	+26.9 ± 0.19
Cy3 BHGCA ALN NP	209.7 ± 1.0	+27.68 ± 0.20

Table 2. Size and zeta potential of Cy3-BHGCA and Cy3-BHGCA-BALN nanoparticle.

4.3 Binding affinity towards HA

Mixture of three different molar ratios of hydroxyapatite to nanoparticle were incubated in both Cy3-BHGCA-BALN and Cy3-BHGCA nanoparticle suspension each of 12mL at 50µg/mL concentration. Molar ratio of nanoparticle to HA was listed in the Figure 14b. The unbound nanoparticle at different times points as 5 min, 10 min, 15 min, 30 min, 1 hr, 3hr, 6hr, 9hr, 1day, 2days and 3days was calculated by measuring the fluorescence of the supernatant after centrifugation and obtaining its equivalent concentration from the standard curve from figure.

The percentage binding was calculated using the given formula. At 10mg, 20mg and 30mg of HA the binding was limited up to 40% after 3 days. The experiment was repeated with higher

concentrations of HA. The binding percentage for these concentrations was remarkably higher achieving 95% binding in 24 hours.

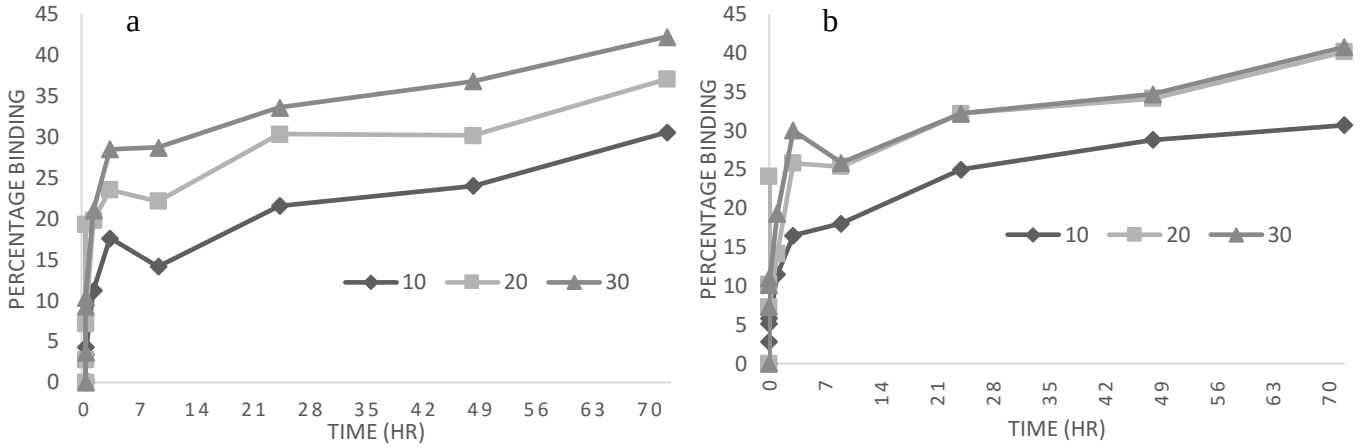

Figure 14. Binding affinity of a) Cy3-BHGCA and b) Cy3-BHGCA-BALN nanoparticles towards different mass of HA 10mg, 20mg, 30mg

ALN NP to HA ratio	
10 mg HA	$1 : 0.13 \times 10^{6}$
20 mg HA	$1 : 0.26 \times 10^{6}$
30 mg HA	$1 : 0.39 \times 10^{6}$
NP only to HA molar ratio	
10 mg HA	$1 : 0.17 \times 10^{6}$
20 mg HA	$1 : 0.35 \times 10^{6}$
30 mg HA	$1 : 0.53 \times 10^{6}$

Table 3. Molar ratios for binding affinity of Cy3-BHGCA and Cy3-BHGCA-BALN nanoparticles towards different mass of HA 10mg, 20mg, 30mg

The above graph (Figure 12a) depicting the binding kinetics of both the nanoparticles are similar with a higher binding at the highest of the three volumes of HA which is 30mg. The experiment is hence repeated by increasing the molar ratio of nanoparticle to HA and the obtained results are shown in the Table 3 below.

NP Only	HA mass (mg)			
Time (hr)	0	50	100	200
	0.25	39.041	44.491	51.756
	1	58.568	64.262	73.169
	3	71.604	77.921	88.274
	6	86.387	88.216	93.165
	24	96.677	94.165	96.420

Table 4. Binding affinity data of Cy3-BHGCA nanoparticles towards different mass of HA.

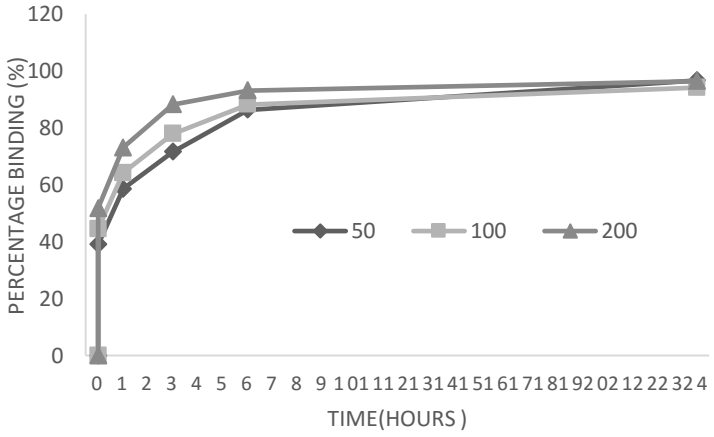

Figure 15. Binding affinity of Cy3-BHGCA nanoparticles towards different mass of HA 50mg, 100mg, 200mg

The increased HA in the molar ratio improved the binding kinetics with a rapid fall in the concentration of nanoparticles in the supernatant. More than 50% of binding was possible within an hour of incubation proving the affinity of both the nanoparticles' affinity towards the bone material mimicking hydroxyapatite. The graph for binding percentage of each nanoparticle is shown in the Figure 15 and 16.

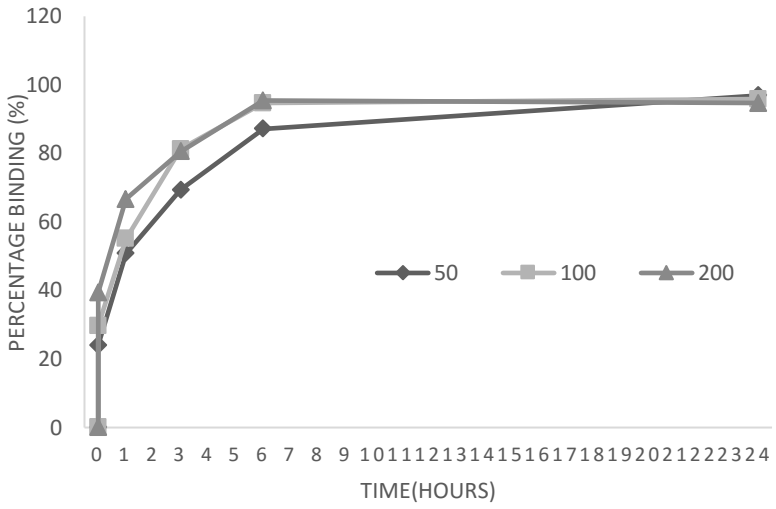

Figure 16. Binding affinity of Cy3-BHGCA-BALN nanoparticles towards different mass of HA 50mg, 100mg, 200mg

Figure 17 shows the comparison between both types of nanoparticle at each concentration. The nanoparticle with alendronate seems to be saturated first in 100mg and 200mg HA volumes, while remaining same for 50mg HA.

ALN NP	HA mass (mg)			
Time (hr)	0	50	100	200
	0.25	24.039	29.690	39.430
	1	50.785	55.075	66.674
	3	69.345	81.263	80.583
	6	87.158	94.696	95.425
	24	96.883	95.856	94.677

Table 5. Binding affinity data Cy3-BHGCA-BALN nanoparticles towards different mass of HA

ALN NP to HA ratio	
50 mg HA	$1 : 1.65 \times 10^{6}$
100 mg HA	$1 : 3.3 \times 10^{6}$
200 mg HA	$1 : 6.6 \times 10^{6}$
NP only to HA molar ratio	
50 mg HA	$1 : 2.4 \times 10^{6}$
100 mg HA	$1 : 4.8 \times 10^{6}$
200 mg HA	$1 : 9.6 \times 10^{6}$

Table 6. Molar ratios for binding affinity of Cy3-BHGCA and Cy3-BHGCA-BALN nanoparticles towards different mass of HA 10mg, 20mg, 30mg

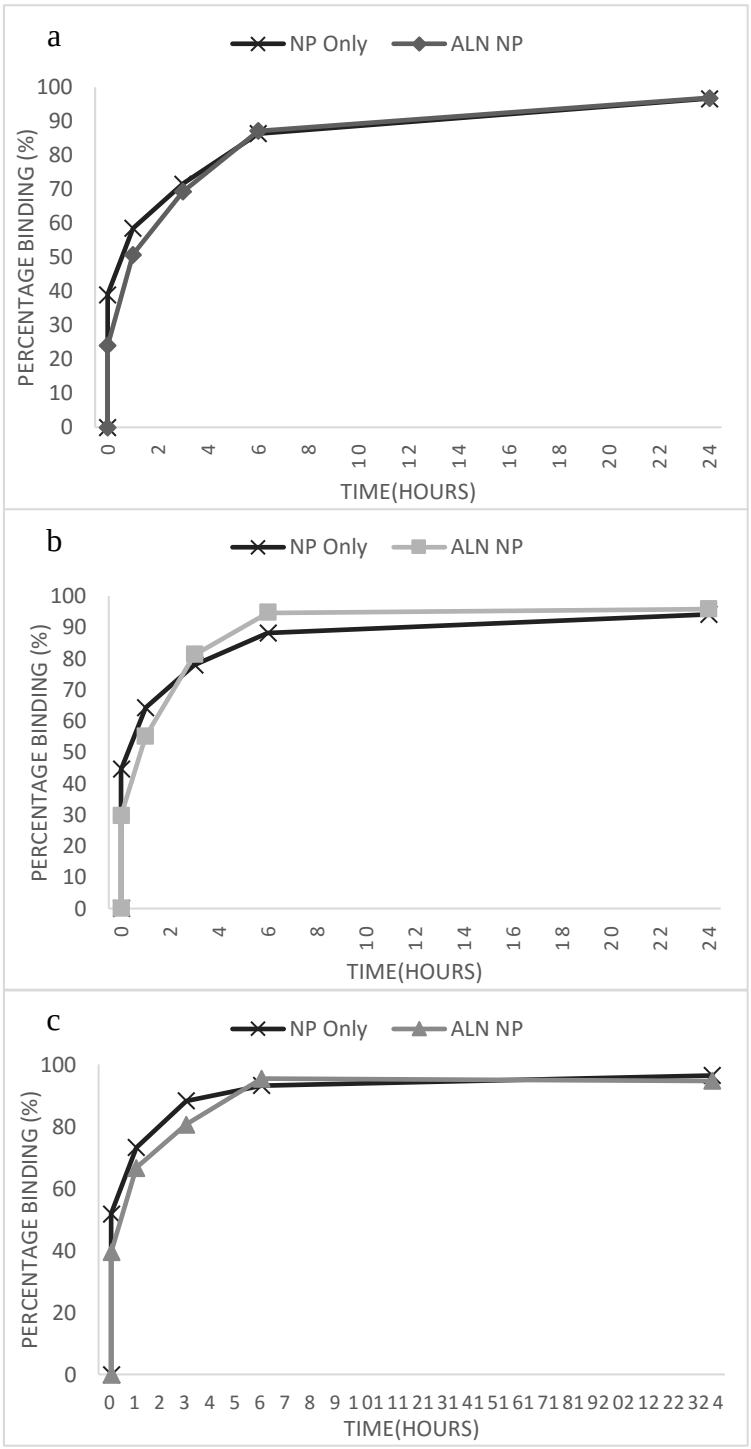

Figure 17. Binding affinity of Cy3-BHGCA and Cy3-BHGCA-BALN nanoparticles towards different mass of HA a) 50mg b) 100mg c) 200mg

The Cy3 BHGCA nanoparticle is quenched with biotin to study the effect of avidin contributing to the stickiness of the nanoparticle resulting in binding to HA. The binding affinity experiment is repeated to compare binding between Cy3 BHGCA BALN and Cy3 BHGCA Biotin. The results of the binding affinity experiment are shown in the following plot.

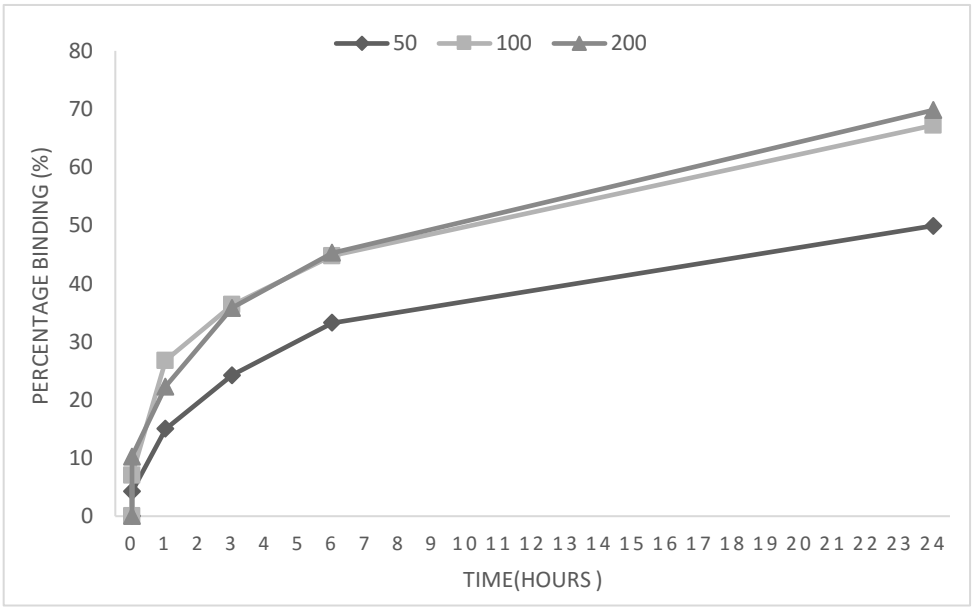

Figure 18. Binding affinity of Cy3-BHGCA-Biotin nanoparticles towards different mass of HA 50mg, 100mg, 200mg

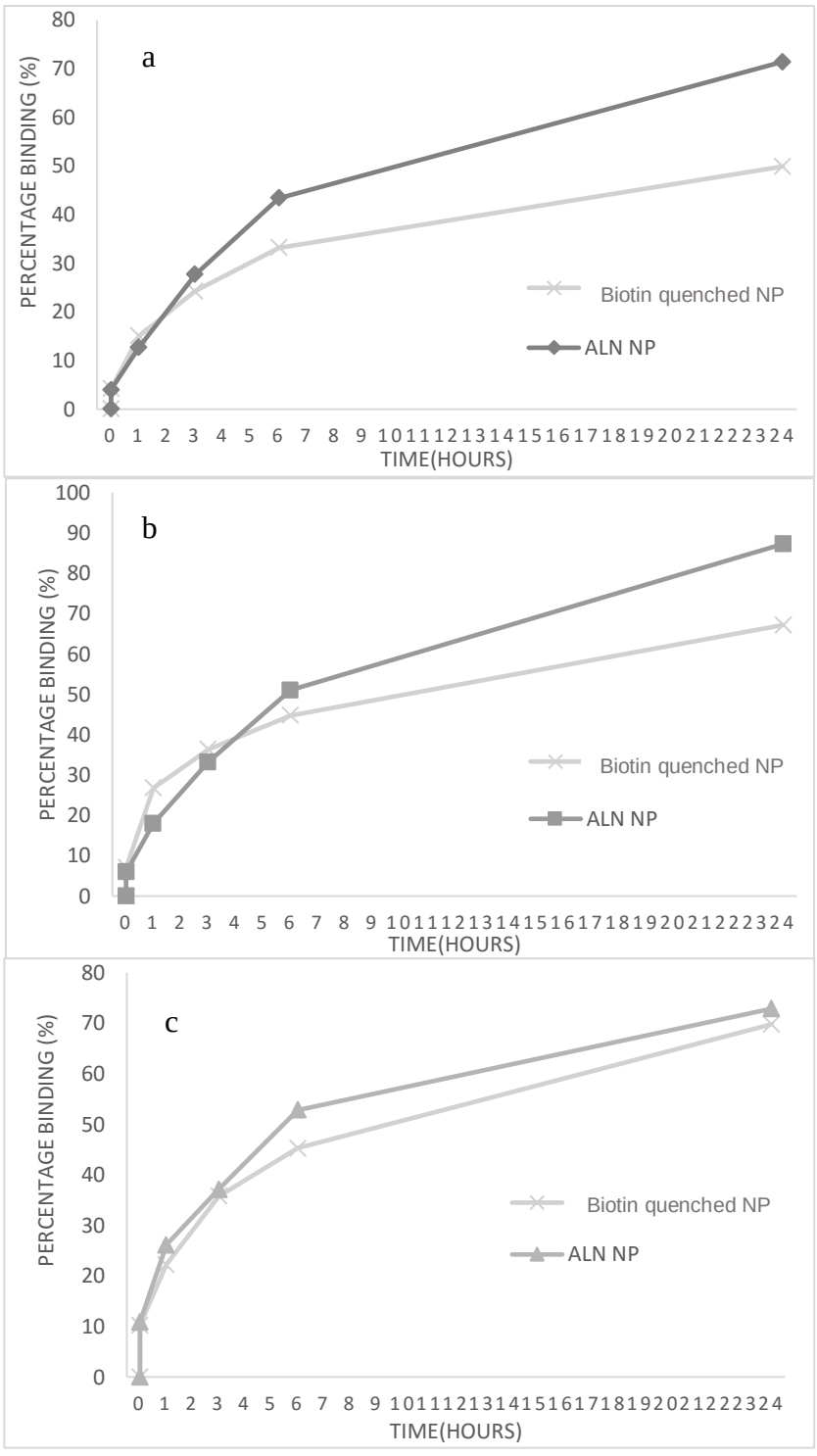

Figure 19. Binding affinity of Cy3-BHGCA BALN and Cy3-BHGCA-Biotin nanoparticles towards different mass of HA a) 50mg b) 100mg c) 200mg

4.4 FTIR analysis

To understand the synthesis chemistry and to analyze the bonds between the molecules within the prepared nanoparticles FTIR studies was done. To study the biotinylation of alendronate, Biotinylated alendronate and Alendronate only samples are analyzed using FTIR. FTIR plot comparing ALN and BALN is shown in the figure x as follows.

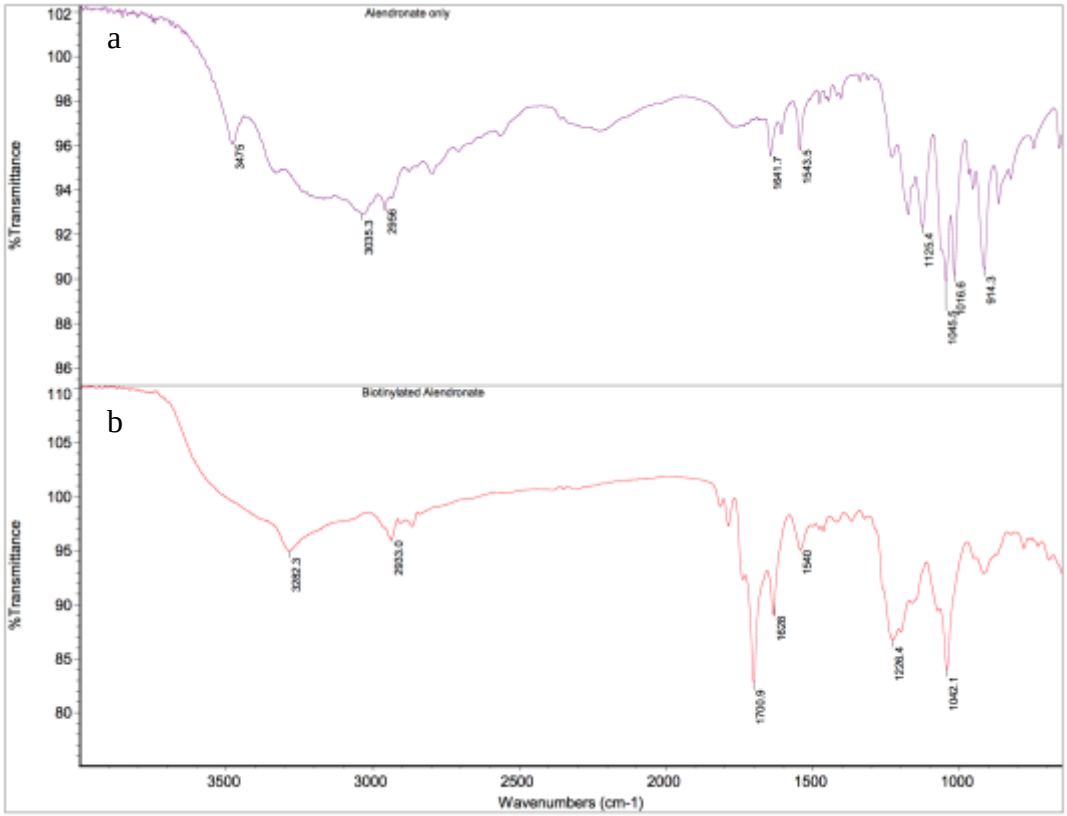

Figure 20. FTIR spectrum of a) Alendronate only and b) Biotinylated alendronate

FTIR studies on Cy3 HGC, Cy3 BHGCAB and Cy3 BHGCA BALN, all three variants of nanoparticles are shown in the following figures. These curves signify the synthesis chemistry and act as control for the analysis of the binding affinity HA samples.

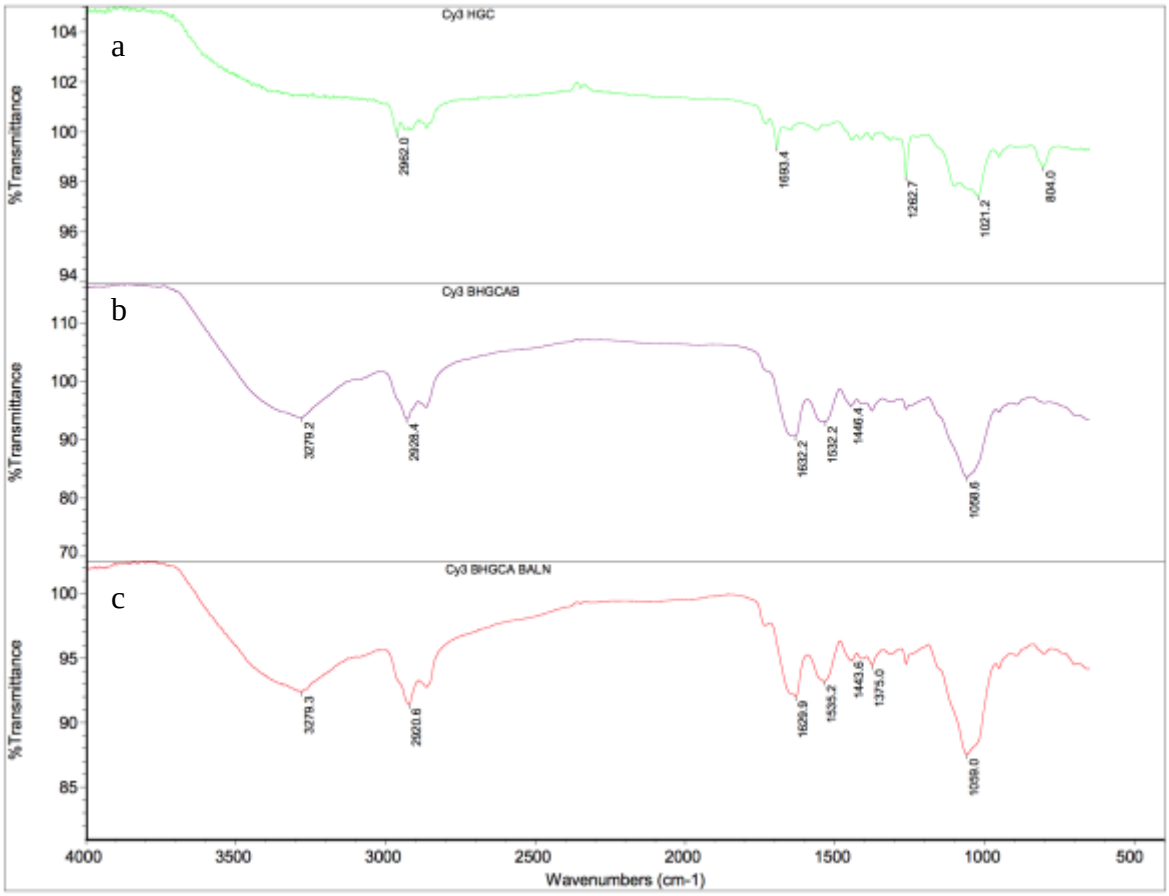

Figure 21. FTIR spectrum of a) Cy3 HGC, b) Cy3 BHGCAB and c) Cy3 BHGCA BALN nanoparticles.

To study the binding chemistry of the nanoparticles to HA, FTIR analysis is conducted. The air-dried 200mg HA sample from binding affinity experiment was studied. The FTIR analysis for each type of nanoparticles with HA and nanoparticle controls is shown in Figures 22 to 24.

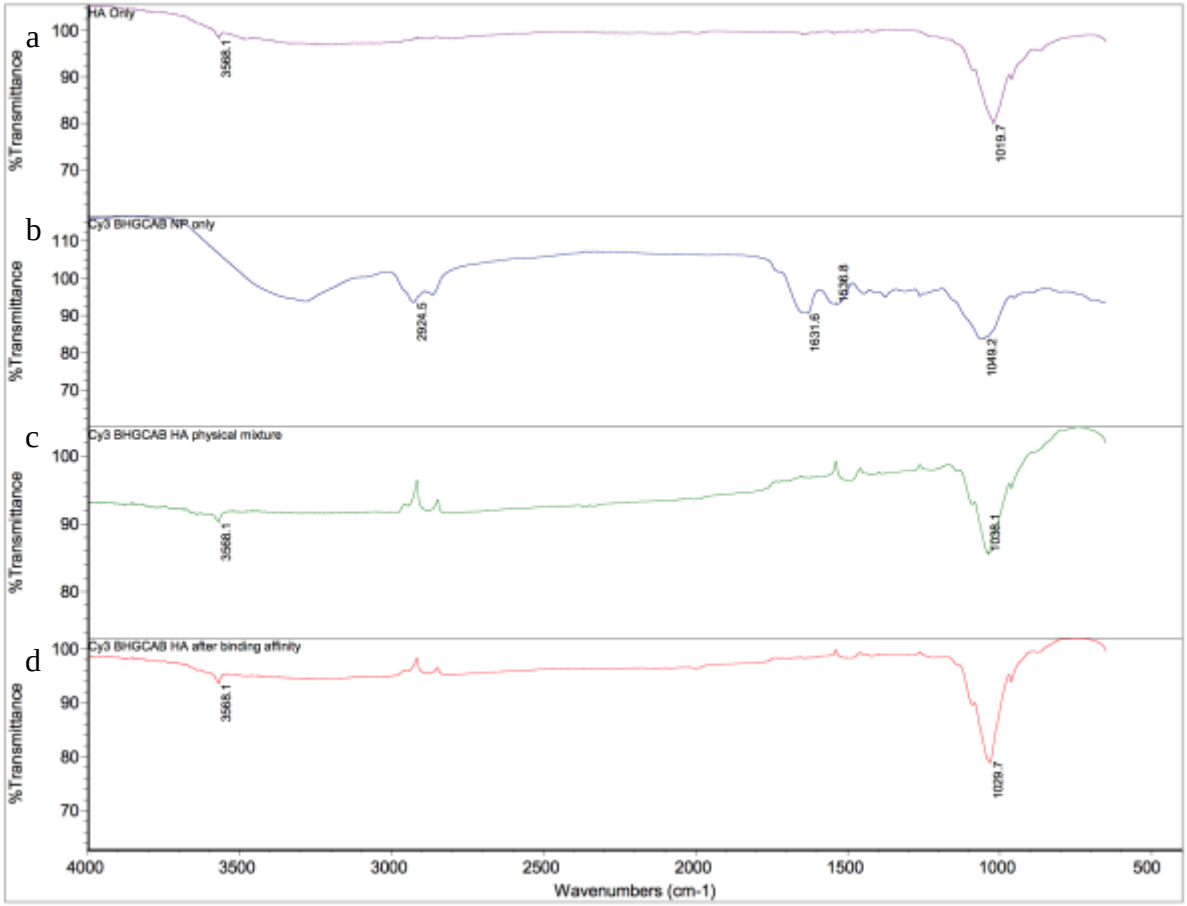

Figure 22. FTIR spectrum of Cy3 BHGCAB nanoparticles in HA studies. Comparison of a) Hydroxyapatite only, b) Cy3 BHGCAB NP only c) Physical mix of a and b d) chemically bound a and b.

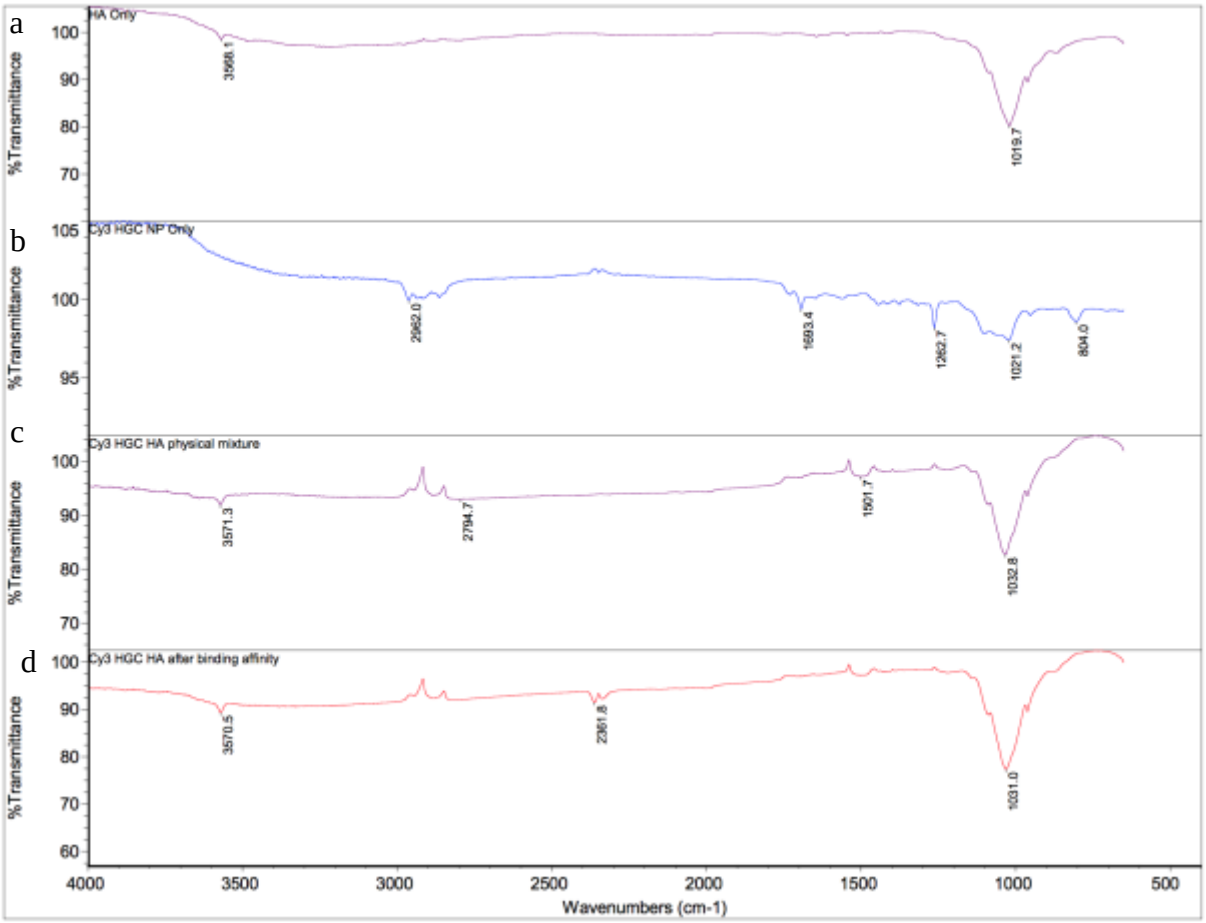

Figure 23. FTIR spectrum of Cy3 HGC nanoparticles in HA studies. Comparison of a) Hydroxyapatite only, b) Cy3 HGC NP only c) Physical mix of a and b d) chemically bound a and b.

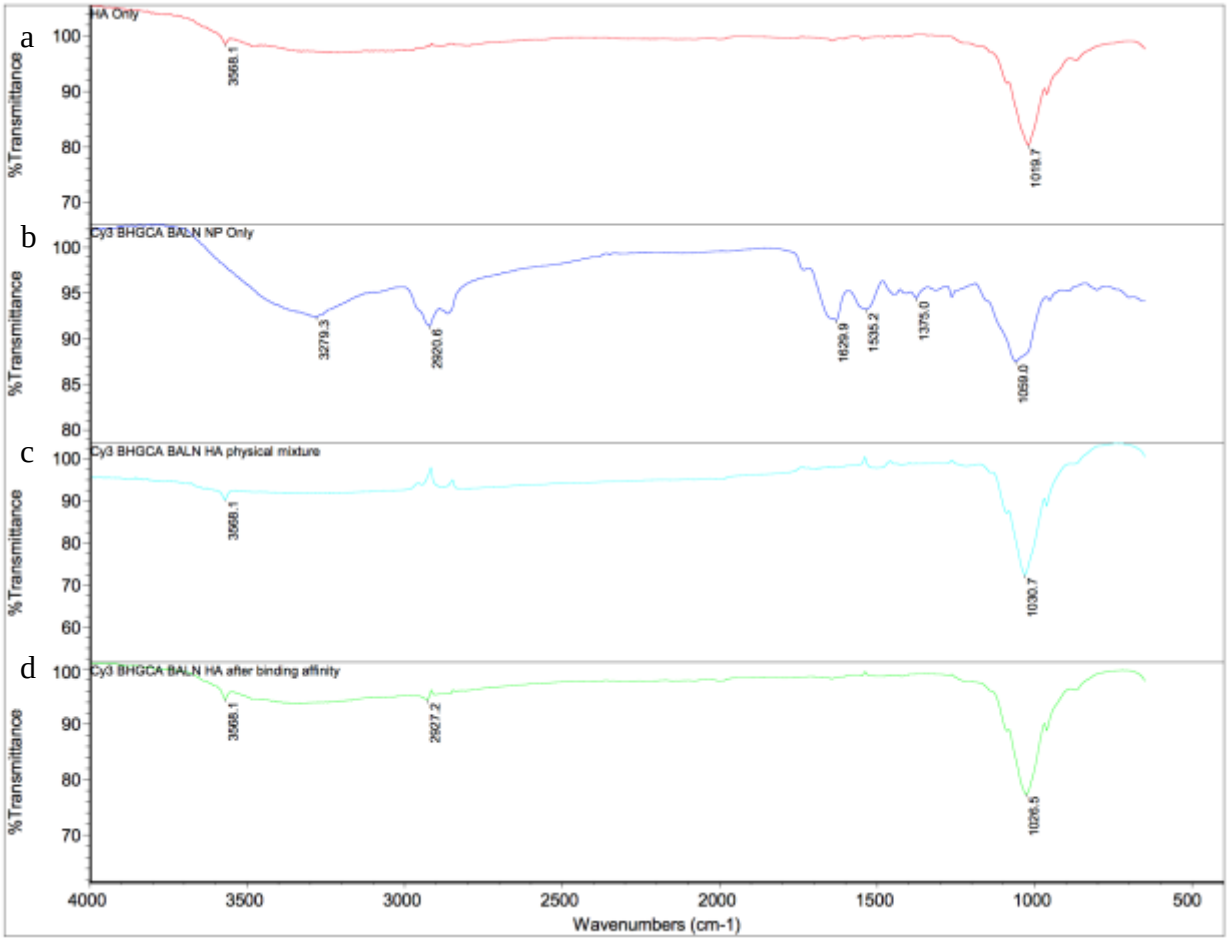

Figure 24. FTIR spectrum of Cy3 BHGCA BALN nanoparticles in HA studies. Comparison of a) Hydroxyapatite only, b) Cy3 BHGCA BALN NP only c) Physical mix of a and b d) chemically bound a and b

4.5 Additional Experiments

4.5.1 Preparation of DOXO loaded HGC

To study the loading efficiencies of different concentration of DOXO in HGC the encapsulation of DOXO in HGC was carried out at 1:15 and 1:10 (DOXO:HGC) molar ratios. Reaction mixture was prepared on the first day of encapsulation. A 250mL Round bottom flask held by a stand inside the hood with a 1000mL beaker placed below for safety was made ready.

To the round bottom flask 20mL of DMSO was added, followed by the slow addition of 70mg of HGC conjugate powder (without touching the wall of the flask). The solution can stir for an hour using stirring bar. DOXO stock solution from the -20°C freezer was taken and defrosted using water bath at 37°C and the required concentration of DOXO in DMSO dilution is made, which is 1.33mL of 3.5mg/mL of DOXO solution for 1:15 and 2mL of 3.5mg/mL of DOXO solution for 1:10. The solution was added drop by drop in DMSO Dendrimer solution in the respective beakers. After stirring for 5 hours, 50 mL of HPLC water was added (1:2.5 mass ratio for DMSO to water).

The DOXO/HGC solution was moved to dialysis cassette with a molecular weight cut-off threshold of 3.5kDa and capacity of 25mL. A total of 6 cassettes were used with 23mL of solution in each. Medium was changed twice for two hours and dialyzed overnight for two days. After dialysis, the sample was removed from cassettes and sent for freeze drying for another two days. The sample was ground to a fine powder after the freeze-dried sample obtained.

DOXO:HGC mass/molar ratio	1:15	1:10
Input HGC	70mg	70mg
Final weight of sample after grinding	26mg	50mg
Yield	37.1%	71.4%

Table 7. Yield efficiency assessments for DOXO HGC encapsulation

4.5.1.1 Preparation of doxorubicin solution

Doxorubicin (DOXO), an orange colored, fluorescent, highly toxic and commonly used anticancer drug stored in -20°C freezer in a clear glass vial inside a larger 20mL Disposable santillation vials, was removed and weighed for 10mg. The powder's sticky nature makes weighing hard, therefore a microspatula was used instead of a scoop due to the small size of vial that contained DOXO.

To prepare the DOXO suspension, a brown Eppendorf tube is first added with 1mL of DMSO. DMSO readily dissolves DOXO and is commonly used as a solvent. Since DOXO is fluorescent a brown Eppendorf tube was used to prevent photobleaching. A 10mg/mL highly concentrated stock solution was made and from that a lesser concentration of 5mg/mL was made and stored -20°C freezer for further use, e.g. encapsulation of the drug in a suitable carrier or obtaining standard curve in media.

4.5.1.2 Standard curve of DOXO in DMSO:HCl (10:2, v/v)

A standard curve of DOXO in DMSO : 0.1M HCl (10:2, v/v) was obtained by adding different concentrations of DOXO in the above mentioned solvent and reading the plates for Fluorescence emission at 580nm with excitation at 488nm.

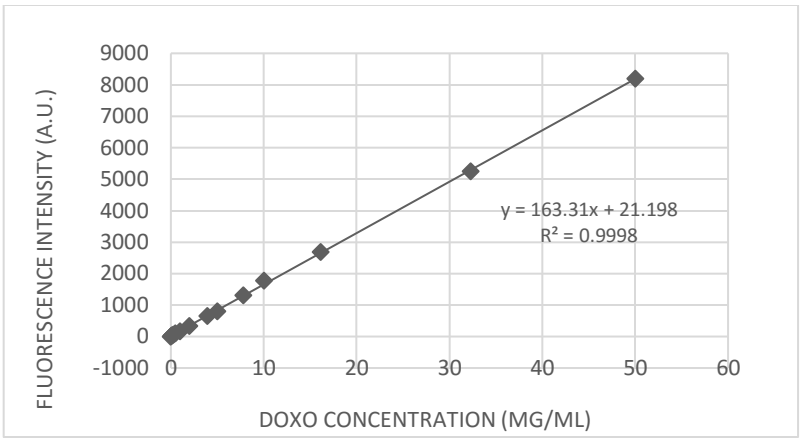

Figure 25. Standard curve DOXO in DMSO:HCl (10:2, v/v)

4.5.1.3 Standard Curve of DOXO in PBS

Like the standard curve obtained for encapsulation efficiency experiments, two standard curves for two different media with varying pH was obtained. A standard curve of DOXO prepared in a mixture of PBS (pH 7.4) and 0.1M HCl (10:2, v/v) was obtained by adding different concentrations of DOXO in the above-mentioned solvent and reading the plates for Fluorescence emission at 580nm with excitation at 488nm. Similarly, standard curve of DOXO in a mixture of Phosphate buffer (pH 6.5) and 0.1M HCl (10:2, v/v) was obtained.

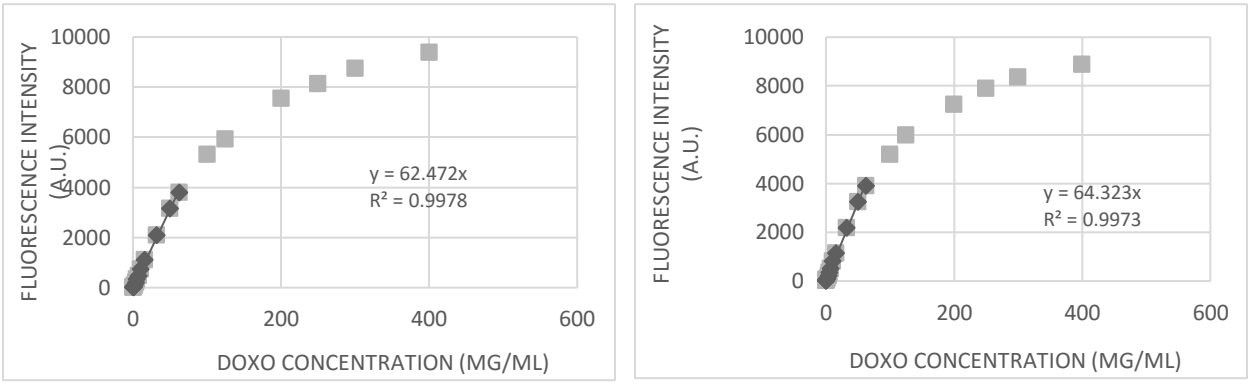

Figure 26. Standard concentration curve for a) PBS pH b) 7.4 Phosphate Buffer pH 6.5

4.5.1.4 Encapsulation efficiency

To measure the encapsulation efficiency and loading capacity of both ratios of the DOXO loaded HGC, an efficiency assessment was carried out. First, 2mg of the DOXO-HGC complex was added to 2mL of 0.1M HCl, followed by the addition of 8mL of DMSO. Using the plate reader, Fluorescence emission at 580nm with excitation at 488nm was measured and from the values of plate reader and standard curve of DOXO, both encapsulation efficiency and loading capacity is calculated.

DOXO:HGC molar ratio	1:10	1:15
DOXO concentration (µg/mL)	11.98	12.18
Amount of DOXO in 10 mL solution (µg)	119.85	121.76
Total amount of DOXO (µg)	2996.28	1582.92
Amount of polymer in 10 mL solution (µg)	1880.15	1878.24
Encapsulation efficiency	65.14%	22.61%
Loading efficiency	6.37%	6.48%

Table 8. Encapsulation efficiency of DOXO encapsulated HGC nanoparticles at 1:10 and 1:15 (DOXO:HGC) ratios

Loading content evaluation:

$$LC\% = \frac{W_{DOXO\ in\ micelles}}{W_{loaded\ micelles}} \quad (4)$$

Encapsulation efficiency:

$$EE\% = \frac{W_{DOXO\ in\ micelles}}{W_{feed\ DOXO}} \times 100 \quad (5)$$

From Table 5 we find that the DOXO:HGC molar ratio of 1:10 has a better Encapsulation efficiency and loading Content, hence the release experiments were conducted for 1:10 sample.

4.5.2 DOXO release kinetics

Studying the release kinetics of a novel carrier is of crucial weight to illuminate the detailed transport mechanism, and it is critical to bridge the gap between the macroscopic data and the transport behavior at the molecular level[59]. To study the DOXO release from HGC at two different pH conditions (7.4 and 6.5), 4mg of DOXO-HGC was first added to 6mL of each type of Buffer. The solution was put in a dialysis tube (10kDa MWCO). The dialysis bag containing the sample was put in a 40mL buffer solution with constant stirring with a stirring bar (dialysis bag should be avoided from contact with stirring bar as it might damage the membrane). Different time points were chosen: 5 min, 15 min, 30 min, 45 min, 60 min, 75 min, 90 min, 2 hr, 4 hr, 6 hours, 1 day, 2 days, 3 days. At each time point 3mL of sample from medium was removed and same volume of buffer was added again as a replacement. Using Plate reader at Fluorescence emission at 580nm and excitation at 488nm the amount of DOXO released was calculated.

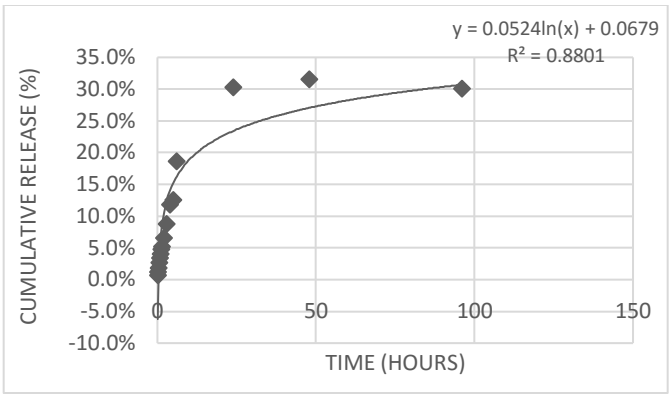

Figure. 27. Cumulative release of doxorubicin from HGC at pH 7.4.

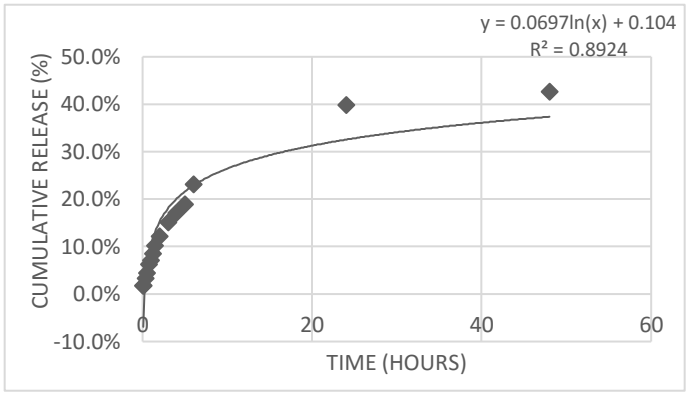

Figure. 28. Cumulative release of doxorubicin from HGC at pH 6.5.

In case of Phosphate buffer 40% of DOXO was released within 24 hours. Thus supporting the 1:10 ratio of DOXO:HGC is optimal drug loading ratio for DOXO HGC drug delivery model.

4.5.3 Delivery of DOXO-loaded HGC nanoparticles to 4T1 murine carcinoma cells

4.5.3.1 Preparing Cell Culture Medium for 4T1 murine carcinoma cells

The basic nutrients to support fastidious or mutant growth requirements for a cell in vitro were obtained from complete medium. It was made with 10% Fetal bovine serum (FBS) and 1% of antibiotics, in this case Pen strep. To 500mL of Serum free DMEM (low glucose), 50mL of

FBS and 5mL of Pen strep were added to make the complete media. The cell culture experiments were kindly performed by Weiyi Li.

4.5.3.2 Cell Plating

The density of 4T1 cancer cells in tissue culture polystyrene plates were checked by viewing at 10x magnification under an inverted microscope with phase contrast mode. If the density of the cells was high with 100% confluence they were required to be split. To split the cells, the medium was aspirated and rinsed twice with PBS (5mL) followed by addition of 2mL trypsin-EDTA and incubation 37°C for 5 minutes. After the cells become visibly detached from the bottom of the dish, 3mL of complete medium were added, making the total volume 5mL, and cells were immediately transferred to Falcon tubes and centrifuged 2400 rpm for 5 minutes. Tissue culture (TC) plates were used in this case as 4T1 cells require a hydrophilic surface to attach. To each 10cm TC plate, 10mL of complete medium were first added. After the medium was aspirated from the Falcon tube containing the cell pellet, 400µL of complete medium was added and the cells are gently mixed. A 100µL aliquot of cell suspension was added to each 10cm plate already containing complete medium, and the plate was gently swirled before being placed in the 37°C incubator.

4.5.3.2 Adding Nanoparticles to the plated cells

The plated cells were checked for cell density and taken to the biosafety cabinet from the incubator. The old medium was aspirated and washed twice with PBS. Fresh medium containing the nanoparticles was added to the plate, and the plate was placed back in the incubator. Similarly, all other plates were treated with respective nanoparticles in appropriate concentration.

4.5.3.3 Freezing of cells

The cells were prepared and frozen for future usage. A 2mL cryotube was labeled with cell line and other information. Total volume of 1mL of cell suspension was prepared, which included 200 µL of FBS, 750 µL of complete medium containing cells trypsinized from a confluent plate of 10 cm plate, and 50 µL of dimethylsulfoxide (DMSO). The vial was quickly transferred to a cooler box containing isopropanol before being placed in a -80°C freezer.

4.5.3.4 Cytotoxicity study: MTS assay

Cytotoxicity of the following three different samples was studied using MTS (3-(4,5-dimethylthiazol-2-yl)-5-(3-carboxymethoxyphenyl)-2-(4-sulfophenyl)-2H-tetrazolium) assay: HGC/DOXO, free DOXO. Each sample at different concentration was studied for its toxicity against the 4T1 murine breast carcinoma cell line. The concentration of each sample was decided by the DOXO content in each carrier, i.e. Free DOXO Molarity was used as a control for different concentration calculation for each nanoparticle used under cytotoxicity tests. Specifically, 0.01, 0.1, 1, 3, 10, 30 are the Molarities for Free DOXO in µM. All samples were prepared in serum free DMEM media. 4T1 cells cultured in 10cm plates were treated with either free DOXO or DOXO-loaded Nanoparticles for up to three days. At each time point, MTS reagents were added to the treated cell samples. Cells were then incubated for 3.5 hours at 37°C and 5% CO_2. The supernatant in each well was transferred to a different 10 cm plate and is diluted with water at 1:3 ratio before being pipetted a new well of a 96 wells plate. Absorbance at 490nm was obtained using the Tecan plate reader.

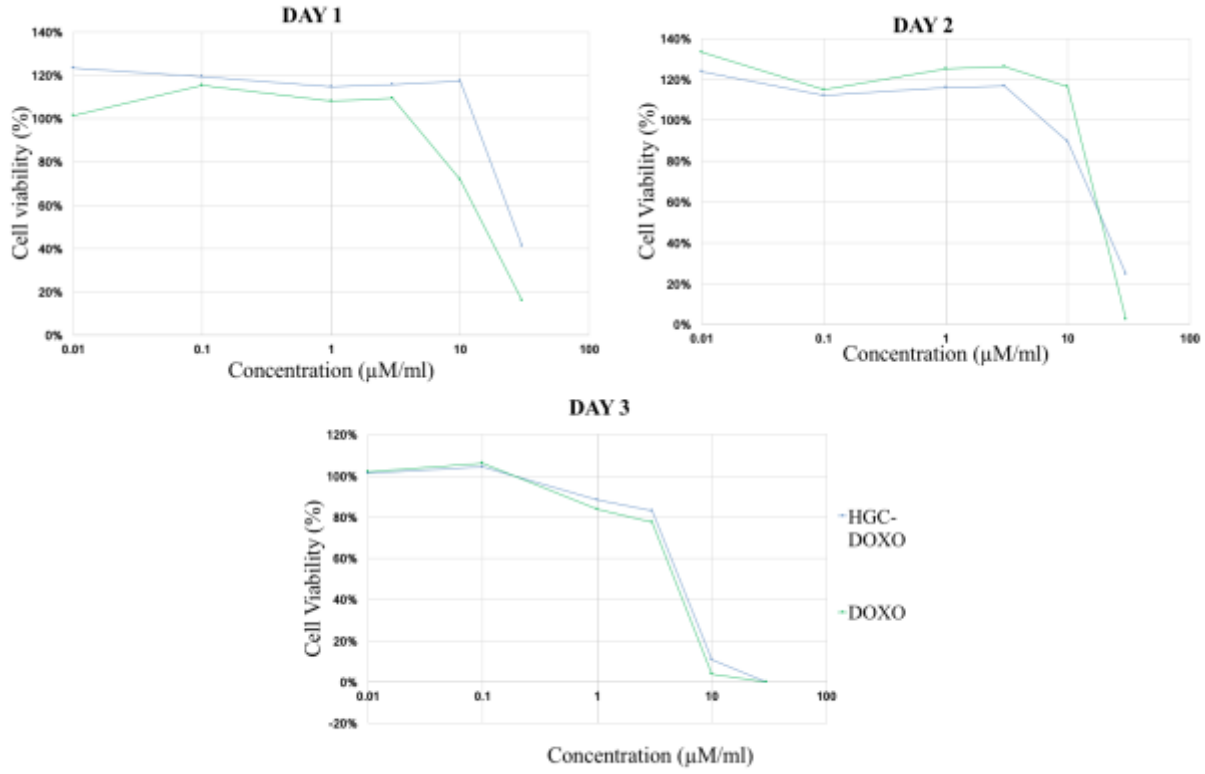

Figure 29. MTS data plots: Day 1 cells were treated with two different treatments - HGC-DOXO, and free DOXO as a control. Free DOXO and HGC/dendrimer begin to show signs of cell cytotoxicity around 10µM. HGC exhibits cell cytotoxicity around 30µM. Overall, cells were still relatively intact.

A few wells were specifically incubated for imaging after MTS, the control wells with cells in complete medium and cells treated with highest concentration of respective nanoparticles were chosen for imaging purposes i.e. 30µM DOXO equivalent nanoparticle treated wells. Fixing and Nucleus immunofluorescence staining was done to image these cells under microscope. The sample permeabilization with Triton was carried out followed by Alexa Fluor 488 and DAPI with PBS used to rinse twice between each step. Morphology of 4T1 cells treated for 3 days each imaged

using fluorescence microscopy imaging visualizing nucleus (blue) and green (cytoskeleton) by mentioned staining.

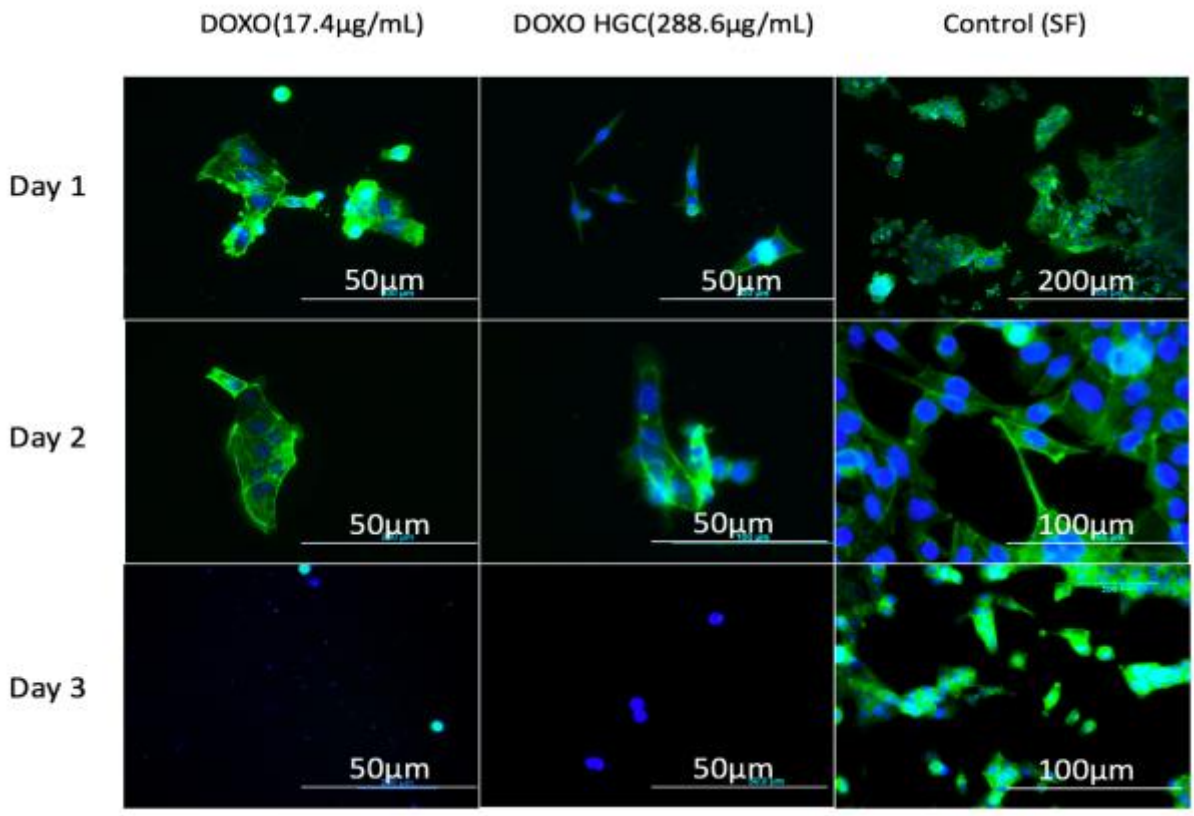

Figure 30. Morphology study imaging showing fluorescence microscopy images of 4T1 cells after 1, 2 or 3 days of incubation with either free doxorubicin or DOXO-loaded nanoparticles. Untreated cells were used as control. Cells were visualized in the blue (nuclei) and green (cytoskeleton) channels.

Chapter 5 Discussion

In our studies, we have: 1) shown that HGC nanoparticles is formed to micelle structures. 2) These nanoparticles are labelled using a fluorescent marker for imaging and quantification studies. 3) Biotin-avidin interaction was successfully used for nanoparticles surface functionalization with alendronate, a bisphosphonate as a calcification targeting probe for targeted theranostics. 4) Significant binding towards hydroxyapatite that mimics cancer microcalcified regions in tumor environments. Several studies have shown that HGC nanoparticles through enhanced permeability have efficient delivery properties for tissue targeting in vivo and in vitro[29,60–63]. In addition to subcellular size of HGC, biocompatibility and biodegradability, a crucial property of surface functionalization owing to presence of side chains is the key behind this study. Here, we report a novel application of HGC in targeting breast cancer microenvironment and show that implementation of HGC-alendronate, making targeted, detectable and imageable nanoparticles that could obtain biological activities like tracking of calcified regions.

5.1 Physiochemical properties

The nanoparticles by default did not have a fluorescent signature and thus Cy3 labelling was done. Since Cy3 is a red fluorescent drug the nanoparticle appeared in a bright pink color after synthesis. The nanoparticles when stored and used for characterization were maintained in the dark. In contrast with HGC nanoparticles, Cy3 BHGCA and Cy3 BHGCA BALN nanoparticles are readily soluble in HPLC grade water. A perfectly homogeneous suspension was possible with just 6 minutes of bath sonication and probe sonication each. This should be due to the presence of biotin and avidin attached to surface of the micelles. The freeze-dried nanoparticles were easier to

grind unlike BGC and BGCA. The micellarization by addition of a hydrophobic component could be the reason behind.

5.2 Size and Zeta potential results

Both Cy3-BHGCA and Cy3-BHGCA-BALN nanoparticles were self-assembled micelles in aqueous environment with diameters of 253.9nm (without ALN) and 210.7 nm (with ALN). In previous study it has been shown that the mean diameter of HGC nanoparticles is 211±14 nm (n=3)[64]. Conjugation of Alendronate to the HGC nanoparticle surface changes the overall particle charge and size both of which might as well affect its migration pattern. The Alendronate modified nanoparticles were smaller than the Cy3 labeled BHGCA possibly because a modification in the physicochemical property of the surface. In wet-chemistry presence of surface modifiers are the most common and known parameters to reduce nano materials particle size. Surface modifiers in this case alendronate is chemically reacted and conjugated to the surface of the nanoparticle but do not physically adhere with the nanoparticle or itself. This could be the reason behind the reduction in the particle size.

DLS offers an ensemble average with decent statistical representation, providing hydrodynamic diameter of particles. The results from DLS obtained agree with previous work. The size range of these nanoparticles is fitting for cellular uptake through endocytosis. Additionally, it is well accepted that nanoparticle systems for in vivo use should remain below 100 nm in diameter to be most effective in systemic delivery[65]. Moreover, splenic filtration accounts for retention of particles >200 nm, due to the 200–500 nm. Our nanomicelles are in a perfect balance in terms of the suitable size range for accumulating in tumor tissue by EPR effects and cellular intake [66].

This result was analogous with the previous study in which the average size of the DOX loaded DOX-hyd-PEG-ALN micelle and DOX loaded DOX-hyd-PEG micelle was approximately 114 nm and 278 nm, respectively. Here, the absolute value of zeta potential of DOX loaded DOX-hyd-PEG-ALN micelle was greater than that of DOX loaded DOX-hyd-PEG micelle, which reduced the aggregation of the micelle.[67]

Zeta potential is an important index of micelle. A more negative surface charge of the micelle was expected due to the presence of ALN segment.[67] There was not much difference in the zeta potential value between the nanoparticles under study, thus there was no significant contribution of alendronate in terms of surface charge.

5.3 Binding affinity

It is well-documented that ALN has a strong affinity with bone tissue because of its hydroxyl group and phosphonate group.[68] To estimate the binding capacity of ALN functionalized Cy3-BHGCA micelle with bone tissue, HA binding assay was carried out. The binding kinetics showed that after 24 hours of incubation, approximately 95% of micelles were bound with HA and reached the plateau within 6 hours.

The Cy3-BHGCA nanoparticle also displayed similar binding. This could be caused by either Avidin, chitosan or biotin. To check if chitosan is contributing to the binding of HA, Cy3-HGC (without biotin and avidin) was tested for its binding affinity. To check if avidin contributes to the binding, Cy3-BHGCA nanoparticle was quenched with biotin to occupy all unoccupied avidin spots thus eliminating avidin from its possibility of interaction with HA.

On comparing binding of Cy3 BHGCA BALN and Cy3 BHGCAB nanoparticles as shown in Figure 17. Binding curves for both types of nanoparticles are distinct at respective concentrations. Alendronate nanoparticles showed higher binding this must be due to biotin occupying the sticky avidin sites. Fall in the binding by addition of biotin supports the possibility of HA crystals sticking to avidin in our nanoparticles as increased biotin did not increase binding so biotin does not contribute to binding. Glycol chitosan might also be playing a role in HA binding.

Chitosan Addition modulated and aided assembly of nHA particles onto itself Abundance of free amino groups on chitosan is reactive (Phosphorylation) and soluble as function of pH. Preparation by Physical binding or Co-precipitating both phases chemically. Chitosan interacts with inorganic ions owing to its hydrophobic and reactive nature in aqueous solution.[69]

5.4 FTIR analysis

Absorption peaks from FTIR spectrum represents fingerprints of synthesized nanoparticles and binding chemistry. The Characteristic peak of Alendronate include N-H stretching at 3500cm^{-1} and C-N stretching between 1100 and 900 cm^{-1}. Biotinylated alendronate spectrum showed three distinct band measured at 1666, 1541 and 1555 cm^{-1}, these bands can be assigned to amide I (C=O stretch), amide II (N-H bending) and amide III.

On comparison of the infrared spectrum of all variants of nanoparticles Cy3 HGC made by Weiyi Li, Cy3 BHGCAB and Cy3 BHGCA BALN, presence of amide peaks between 1632 to 1443 cm^{-1} in BHGCA nanoparticles represents biotinylation at amino functional groups. Additionally, O-H stretch peaks at 3550 to 3200 cm^{-1}, OH bending of Carboxylic group from 1440

to 1375 cm^{-1} and alkyl C-H stretch between 2950 to 2850 cm^{-1} from glycol chitosan's functional group, Cy3 and biotin.

The characteristic peak of hydroxyapatite was visible for O-H stretching at 3572 cm^{-1} and PO_4 vibrations between 1150 and 850 cm^{-1}. Hydroxyapatite binding to each nanoparticle was studied by comparing HA Nanoparticle physical mixture and chemical binding from sample from palette after binding affinity experiment. Though the peaks are weak because of high HA to nanoparticle ratio peaks at 1530 cm^{-1} shows the presence of nanoparticles in all three variants' physical and chemical mixture.

Principal intermolecular interaction between ALN and HA, which constitutes the ALN-HA composite, is an electrostatic interaction. This electrostatic interaction begins in the relatively large partial negative charge that both elements of ALN share and the positive charge of the calcium atoms of HA. The amino nitrogen atom bears one electron pair, resulting in a partial negative charge. The oxygen atoms of the phosphate groups of ALN have partial negative charges.[70]

Hydroxyapatite crystal is constituted by layers by layers of phosphate and hydroxide groups intercalated with layers of calcium ions. The amino group in the end of the side chain in the isolated molecules is important for intramolecular bond. The amino nitrogen forms a OH-N hydrogen bond with a tridentate binding with calcium atoms. The same type of binding is seen in chemisorption of BPs to bone mineral.[70]

Chapter 6 Conclusion

In this study, Hydrophobically modified glycol chitosan nanomicelles was modified with alendronate through avidin biotin interaction strategy where HGC molecules were biotinylated either at the amine groups ($-NH_2$) or the hydroxyl groups (-OH) on the chitosan backbone. Three variants of GC based nanoparticle systems were successfully synthesized with particle diameters and surface charges measured. The average diameter was 254.0 ± 0.43 nm and 209.7 ± 1.0 nm for Cy3-BHGCA and Cy3-BHGCA-BALN nanoparticles respectively. The average surface charge was +26.9 ± 0.19 mV and +27.68 ± 0.20 mV for Cy3-BHGCA and Cy3-BHGCA-BALN nanoparticles respectively. The effective diameter of alendronate conjugated nanoparticle was approximately 40nm less than the nanoparticle without alendronate attached to it. The surface charge remained similar in both the nanoparticles.

Cyanine 3 was conjugated to HGC to aid in the visualization of nanoparticles. The prepared nanoparticle was suspended in HPLC water and binding kinetics is measured at different time points from 15 minutes to 24 hours. Cy3 labelled BHGCA and BHGCA BALN nanoparticles displayed similar binding of up to 95% binding in 24 hours. However, Cy3 BHGCAB nanoparticle showed a lower binding of 68% binding in 24 hours of incubation proving avidin can stick to HA crystals. Also, absence of free avidin resulting in fall in binding signifies alendronate playing a role in binding kinetics of nanoparticles to HA.

This HGC modified with alendronate nanomicelle system may be used for both therapeutic and diagnostic applications as drug delivery vehicle by loading drugs like doxorubicin and imaging contrast agents in the hydrophobic core of the micelles. As a result, the selectivity of the nanocarrier system can be improved and the side effects due to the untargeted theranostics in non-

specific sites can be minimized. Thus, Alendronate conjugated HGC nanoparticle system is a potential candidate for theranostic applications.

Chapter 7 Future work

Next, the binding affinity should be carried out with HGC nanoparticles without avidin and biotin conjugation to verify the affinity of Glycol chitosan polymer and 5ß Cholanic acid towards hydroxyapatite. TEM imaging and NMR studies should be performed for further characterization of our nanoparticles. Cell uptake and cytotoxicity studies should be conducted with tumor and normal cells.

The systems can be co-conjugated with specific tumor targeting biomolecules to improve targeting efficiency using biotin avidin linkage. In vitro tumor targeting will be conducted for investigating tumor selective ability.

Chapter 8 Reference

1. Situ, B. C. I. Cancer Facts. (2015).
2. Siegel, R. L., Miller, K. D. & Jemal, A. Cancer statistics, 2016. *CA. Cancer J. Clin.* **66,** 7–30 (2016).
3. Torre, L. A. *et al.* Global Cancer Statistics, 2012. *Ca- Cancer J. Clin.* **65,** 87–108 (2015).
4. Hanahan, D. & Weinberg, R. A. Hallmarks of Cancer: The Next Generation. *Cell* **144,** 646–674 (2011).
5. Moghimi, S. M., Hunter, A. C. & Murray, J. C. Nanomedicine: current status and future prospects. *Faseb J.* **19,** 311–330 (2005).
6. Chowdhury, M. R., Schumann, C., Bhakta-Guha, D. & Guha, G. Cancer nanotheranostics: Strategies, promises and impediments. *Biomed. Pharmacother.* **84,** 291–304 (2016).
7. DeVita, V. T. & Chu, E. A History of Cancer Chemotherapy. *Cancer Res.* **68,** 8643–8653 (2008).
8. Ron, E. Cancer risks from medical radiation. *Health Phys.* **85,** 47–59 (2003).
9. Muhamad12, I. I., Selvakumaran, S. & Lazim, N. A. M. Designing polymeric nanoparticles for targeted drug delivery system. *Nanomed.* **287,** 287 (2014).
10. Lammers, T., Aime, S., Hennink, W. E., Storm, G. & Kiessling, F. Theranostic Nanomedicine. *Acc. Chem. Res.* **44,** 1029–1038 (2011).
11. Han, K. *et al.* Dual-stage-light-guided tumor inhibition by mitochondria-targeted photodynamic therapy. *Adv. Funct. Mater.* **25,** 2961–2971 (2015).
12. Dadras, P. *et al.* Formulation and evaluation of targeted nanoparticles for breast cancer theranostic system. *Eur. J. Pharm. Sci.* **97,** 47–54 (2017).

13. Weatherall, P. T., Evans, G. F., Metzger, G. J., Saborrian, M. H. & Leitch, A. M. MRI vs. histologic measurement of breast cancer following chemotherapy: Comparison with X-ray mammography and palpation. *J. Magn. Reson. Imaging* **13,** 868–875 (2001).
14. Savic, R., Eisenberg, A. & Maysinger, D. Block copolymer micelles as delivery vehicles of hydrophobic drugs: Micelle-cell interactions. *J. Drug Target.* **14,** 343–355 (2006).
15. Tyrrell, Z. L., Shen, Y. & Radosz, M. Fabrication of micellar nanoparticles for drug delivery through the self-assembly of block copolymers. *Prog. Polym. Sci.* **35,** 1128–1143 (2010).
16. Kataoka, K., Harada, A. & Nagasaki, Y. Block copolymer micelles for drug delivery: design, characterization and biological significance. *Adv. Drug Deliv. Rev.* **47,** 113–131 (2001).
17. Riess, G. Micellization of block copolymers. *Prog. Polym. Sci.* **28,** 1107–1170 (2003).
18. Micelle. *Wikipedia* (2017).
19. Gitsov, I., Lambrych, K. R., Remnant, V. A. & Pracitto, R. Micelles with highly branched nanoporous interior: Solution properties and binding capabilities of amphiphilic copolymers with linear dendritic architecture. *J. Polym. Sci. Part Polym. Chem.* **38,** 2711–2727 (2000).
20. Kwon, S. *et al.* Physicochemical Characteristics of Self-Assembled Nanoparticles Based on Glycol Chitosan Bearing 5β-Cholanic Acid. *Langmuir* **19,** 10188–10193 (2003).
21. Le Garrec, D. *et al.* Poly(N-vinylpyrrolidone)-block-poly(D,L-lactide) as a new polymeric solubilizer for hydrophobic anticancer drugs: in vitro and in vivo evaluation. *J. Control. Release Off. J. Control. Release Soc.* **99,** 83–101 (2004).
22. Polymeric micelles of poly(2-ethyl-2-oxazoline)-block-poly(ε-caprolactone) copolymer as a carrier for paclitaxel. Available at: https://www.researchgate.net/publication/223249073_Polymeric_micelles_of_poly2-ethyl-2-

oxazoline-block-polye-caprolactone_copolymer_as_a_carrier_for_paclitaxel. (Accessed: 18th February 2017)

23. Licciardi, M. *et al.* New folate-functionalized biocompatible block copolymer micelles as potential anti-cancer drug delivery systems. *Polymer* **47,** 2946–2955 (2006).
24. Kumari, A., Yadav, S. K. & Yadav, S. C. Biodegradable polymeric nanoparticles based drug delivery systems. *Colloids Surf. B-Biointerfaces* **75,** 1–18 (2010).
25. Harris, R., Lecumberri, E. & Heras, A. Chitosan-Genipin Microspheres for the Controlled Release of Drugs: Clarithromycin, Tramadol and Heparin. *Mar. Drugs* **8,** 1750–1762 (2010).
26. Duceppe, N. & Tabrizian, M. Advances in using chitosan-based nanoparticles for *in vitro* and *in vivo* drug and gene delivery. *Expert Opin. Drug Deliv.* **7,** 1191–1207 (2010).
27. Lee, S. J. *et al.* Comparative study of photosensitizer loaded and conjugated glycol chitosan nanoparticles for cancer therapy. *J. Controlled Release* **152,** 21–29 (2011).
28. Lalatsa, A. *et al.* Delivery of Peptides to the Blood and Brain after Oral Uptake of Quaternary Ammonium Palmitoyl Glycol Chitosan Nanoparticles. *Mol. Pharm.* **9,** 1764–1774 (2012).
29. Nam, H. Y. *et al.* Cellular uptake mechanism and intracellular fate of hydrophobically modified glycol chitosan nanoparticles. *J. Controlled Release* **135,** 259–267 (2009).
30. Na, J. H. *et al.* Effect of the stability and deformability of self-assembled glycol chitosan nanoparticles on tumor-targeting efficiency. *J. Controlled Release* **163,** 2–9 (2012).
31. Yhee, J. Y. *et al.* Self-assembled glycol chitosan nanoparticles for disease-specific theranostics. *J. Controlled Release* **193,** 202–213 (2014).
32. Park, K. *et al.* Effect of polymer molecular weight on the tumor targeting characteristics of self-assembled glycol chitosan nanoparticles. *J. Controlled Release* **122,** 305–314 (2007).

33. Novoa-Carballal, R., Riguera, R. & Fernandez-Megia, E. Chitosan hydrophobic domains are favoured at low degree of acetylation and molecular weight. *Polymer* **54,** 2081–2087 (2013).

34. Yu, J. *et al.* Fabrication and characterization of nuclear localization signal-conjugated glycol chitosan micelles for improving the nuclear delivery of doxorubicin. *Int. J. Nanomedicine* 5079 (2012). doi:10.2147/IJN.S36150

35. Kim, J.-H. *et al.* Facilitated intracellular delivery of peptide-guided nanoparticles in tumor tissues. *J. Controlled Release* **157,** 493–499 (2012).

36. Pan, Z. *et al.* Amphiphilic N-(2,3-dihydroxypropyl)–chitosan–cholic acid micelles for paclitaxel delivery. *Carbohydr. Polym.* **94,** 394–399 (2013).

37. Yoon, H. Y. *et al.* Glycol chitosan nanoparticles as specialized cancer therapeutic vehicles: Sequential delivery of doxorubicin and Bcl-2 siRNA. *Sci. Rep.* **4,** 6878 (2014).

38. DeSantis, C. E. *et al.* Breast Cancer Statistics, 2015: Convergence of Incidence Rates Between Black and White Women. *Ca- Cancer J. Clin.* **66,** 31–42 (2016).

39. Microcalcification. *Wikipedia* (2015).

40. Henrot, P., Leroux, A., Barlier, C. & Génin, P. Breast microcalcifications: The lesions in anatomical pathology. *Diagn. Interv. Imaging* **95,** 141–152 (2014).

41. Kubíček, V. & Lukeš, I. Bone-seeking probes for optical and magnetic resonance imaging. *Future Med. Chem.* **2,** 521–531 (2010).

42. Cole, L. E., Vargo-Gogola, T. & Roeder, R. K. Bisphosphonate-Functionalized Gold Nanoparticles for Contrast-Enhanced X-Ray Detection of Breast Microcalcifications. *Biomaterials* **35,** 2312–2321 (2014).

43. Ossipov, D. A. Bisphosphonate-modified biomaterials for drug delivery and bone tissue engineering. *Expert Opin. Drug Deliv.* **12,** 1443–1458 (2015).

44. Ehrick, R. S., Capaccio, M., Puleo, D. A. & Bachas, L. G. Ligand-Modified Aminobisphosphonate for Linking Proteins to Hydroxyapatite and Bone Surface. *Bioconjug. Chem.* **19,** 315–321 (2008).

45. Rosales, R. T. M. de, Finucane, C., Mather, S. J. & Blower, P. J. Bifunctional bisphosphonate complexes for the diagnosis and therapy of bone metastases. *Chem. Commun.* 4847–4849 (2009). doi:10.1039/B908652H

46. Sandiford, L. *et al.* Bisphosphonate-Anchored PEGylation and Radiolabeling of Superparamagnetic Iron Oxide: Long-Circulating Nanoparticles for in Vivo Multimodal (T1 MRI-SPECT) Imaging. *ACS Nano* **7,** 500–512 (2013).

47. Wang, G., Mostafa, N. Z., Incani, V., Kucharski, C. & Uludağ, H. Bisphosphonate-decorated lipid nanoparticles designed as drug carriers for bone diseases. *J. Biomed. Mater. Res. A* **100,** 684–693 (2012).

48. Li, N., Song, J., Zhu, G., Shi, X. & Wang, Y. Alendronate conjugated nanoparticles for calcification targeting. *Colloids Surf. B Biointerfaces* **142,** 344–350 (2016).

49. Torres Martin de Rosales, R. *et al.* Synthesis of 64CuII–Bis(dithiocarbamatebisphosphonate) and Its Conjugation with Superparamagnetic Iron Oxide Nanoparticles: In Vivo Evaluation as Dual-Modality PET–MRI Agent. *Angew. Chem. Int. Ed.* **50,** 5509–5513 (2011).

50. Evans, E. & Ritchie, K. Dynamic strength of molecular adhesion bonds. *Biophys. J.* **72,** 1541–1555 (1997).

51. Avidin-Biotin Interaction. Available at: https://www.thermofisher.com/us/en/home/life-science/protein-biology/protein-biology-learning-center/protein-biology-resource-library/pierce-protein-methods/avidin-biotin-interaction.html. (Accessed: 24th February 2017)

52. Livnah, O., Bayer, E., Wilchek, M. & Sussman, J. 3-Dimensional Structures of Avidin and the Avidin-Biotin Complex. *Proc. Natl. Acad. Sci. U. S. A.* **90,** 5076–5080 (1993).

53. Tarrus, M. *et al.* RGD-avidin–biotin pretargeting to αvβ3 integrin enhances the proapoptotic activity of TNFα related apoptosis inducing ligand (TRAIL). *Apoptosis* **13,** 225–235 (2008).

54. Pierce, Avidin-Biotin Technical Handbook, Thermo Scientific, 2010.

55. White, N. S. & Errington, R. J. Fluorescence techniques for drug delivery research: theory and practice. *Adv. Drug Deliv. Rev.* **57,** 17–42 (2005).

56. *Transmission Electron Microscopy - A Textbook for | David B. Williams | Springer*.

57. ABUBAKAR, I. A. EFFECT OF ACRYLAMIDE GRAFTED POLYETHENE WASTE ON THE PHYSICO-MECHANICAL PROPERTIES OF CONCRETE COMPOSITE. (2015).

58. Li, W. 2015, Biotinylated self-assembled micelles as potential vehicles for targeted anti-cancer drug delivery, State University of New York at Stony Brook.

59. Fu, Y. & Kao, W. J. Drug Release Kinetics and Transport Mechanisms of Non-degradable and Degradable Polymeric Delivery Systems. *Expert Opin. Drug Deliv.* **7,** 429–444 (2010).

60. Kim, J.-H. *et al.* Hydrophobically modified glycol chitosan nanoparticles as carriers for paclitaxel. *J. Controlled Release* **111,** 228–234 (2006).

61. Hwang, H.-Y., Kim, I.-S., Kwon, I. C. & Kim, Y.-H. Tumor targetability and antitumor effect of docetaxel-loaded hydrophobically modified glycol chitosan nanoparticles. *J. Controlled Release* **128,** 23–31 (2008).

62. Min, K. H. *et al.* Hydrophobically modified glycol chitosan nanoparticles-encapsulated camptothecin enhance the drug stability and tumor targeting in cancer therapy. *J. Controlled Release* **127,** 208–218 (2008).

63. Hyung Park, J. *et al.* Self-assembled nanoparticles based on glycol chitosan bearing hydrophobic moieties as carriers for doxorubicin: In vivo biodistribution and anti-tumor activity. *Biomaterials* **27,** 119–126 (2006).
64. Li, T. *et al.* Use of glycol chitosan modified by 5β-cholanic acid nanoparticles for the sustained release of proteins during murine embryonic limb skeletogenesis. *J. Controlled Release* **144,** 101–108 (2010).
65. Conners, C. M., Bhethanabotla, V. R. & Gupta, V. K. Concentration-dependent effects of alendronate and pamidronate functionalized gold nanoparticles on osteoclast and osteoblast viability. *J. Biomed. Mater. Res. B Appl. Biomater.* **105,** 21–29 (2017).
66. Blanco, E., Shen, H. & Ferrari, M. Principles of nanoparticle design for overcoming biological barriers to drug delivery. *Nat. Biotechnol.* **33,** 941–951 (2015).
67. Ye, W. *et al.* Doxorubicin-poly (ethylene glycol)-alendronate self-assembled micelles for targeted therapy of bone metastatic cancer. *Sci. Rep.* **5,** 14614 (2015).
68. Ozcan, I. *et al.* Synthesis and characterization of surface-modified PBLG nanoparticles for bone targeting: in vitro and in vivo evaluations. *J. Pharm. Sci.* **100,** 4877–4887 (2011).
69. Kumar, R., Prakash, K. ., Cheang, P., Gower, L. & Khor, K. . Chitosan-mediated crystallization and assembly of hydroxyapatite nanoparticles into hybrid nanostructured films. *J. R. Soc. Interface* **5,** 427–439 (2008).
70. Neves, M. *et al.* Synthesis, characterization and biodistribution of bisphosphonates Sm-153 complexes: correlation with molecular modeling interaction studies. *Nucl. Med. Biol.* **29,** 329–338 (2002).